

THE CENTERS OF EARLY-TYPE GALAXIES WITH *HST*. IV.
CENTRAL PARAMETER RELATIONS¹

S.M. FABER

UCO/Lick Observatory, Board of Studies in Astronomy and Astrophysics,
University of California, Santa Cruz, CA 95064
Electronic mail: faber@ucolick.org

SCOTT TREMAINE

CIAR Cosmology and Gravity Program, Canadian Institute for Theoretical Astrophysics
University of Toronto, 60 St. George St., Toronto M5S 3H8, Canada
Electronic mail: tremaine@cita.utoronto.ca

EDWARD A. AJHAR

Kitt Peak National Observatory, National Optical Astronomy Observatories²,
P.O. Box 26732, Tucson, AZ 85726
Electronic mail: ajhar@noao.edu

YONG-IK BYUN³

Institute for Astronomy, University of Hawaii, 2680 Woodlawn Dr., Honolulu, HI 96822
Electronic mail: byun@haneul.phy.ncu.edu.tw

ALAN DRESSLER

The Observatories of the Carnegie Institution, 813 Santa Barbara St., Pasadena, CA 91101
Electronic mail: dressler@ociw.edu

KARL GEBHARDT⁴

Department of Astronomy, University of Michigan, Ann Arbor, MI 48109
Electronic mail: gebhardt@astro.lsa.umich.edu

CARL GRILLMAIR⁵

UCO/Lick Observatory, Board of Studies in Astronomy and Astrophysics,
University of California, Santa Cruz, CA 95064
Electronic mail: carl@grandpa.jpl.nasa.gov

¹ Based on observations with the NASA/ESA *Hubble Space Telescope*, obtained at the Space Telescope Science Institute, which is operated by AURA, Inc., under NASA contract NAS 5-26555.

² Operated by AURA under cooperative agreement with the U. S. National Science Foundation.

³ Present address: Institute of Astronomy, National Central University, Chung-Li, Taiwan 32054, R. O. C.

⁴ Present address: UCO/Lick Observatory, University of California, Santa Cruz, CA 95064.

⁵ Present address: Jet Propulsion Laboratory, Mail Stop 183-900, 4800 Oak Grove Drive, Pasadena, CA 91109.

JOHN KORMENDY

Institute for Astronomy, University of Hawaii, 2680 Woodlawn Dr., Honolulu, HI 96822
Electronic mail: kormendy@oort.ifa.hawaii.edu

TOD R. LAUER

Kitt Peak National Observatory, National Optical Astronomy Observatories²,
P.O. Box 26732, Tucson, AZ 85726
Electronic mail: lauer@noao.edu

DOUGLAS RICHSTONE

Department of Astronomy, University of Michigan, Ann Arbor, MI 48109
Electronic mail: dor@astro.lsa.umich.edu

Received _____ ; *Revised* _____

ABSTRACT

We analyze *Hubble Space Telescope* surface-brightness profiles of 61 elliptical galaxies and spiral bulges (hereafter “hot” galaxies). The profiles are parameterized by break radius r_b and break surface brightness I_b . These are combined with central velocity dispersions, total luminosities, rotation velocities, and isophote shapes to explore correlations among central and global properties. Luminous hot galaxies ($M_V < -22$) have *cuspy cores* with steep outer power-law profiles that break at $r \approx r_b$ to shallow inner profiles $I \propto r^{-\gamma}$ with $\gamma \leq 0.3$. Break radii and core luminosities for these objects are approximately proportional to effective radii and total luminosities. Scaling relations are presented for several core parameters as a function of total luminosity. Cores follow a fundamental plane that parallels the global fundamental plane for hot galaxies but is 30% thicker. Some of this extra thickness may be due to the effect of massive black holes (BHs) on central velocity dispersions. Faint hot galaxies ($M_V > -20.5$) show steep, largely featureless *power-law* profiles that lack cores. Measured values of r_b and I_b for these galaxies are limits only. At a limiting radius of 10 pc, the centers of power-law galaxies are up to 1000 times denser in mass and luminosity than the cores of large galaxies. At intermediate magnitudes ($-22 < M_V < -20.5$), core and power-law galaxies coexist, and there is a range in r_b at a given luminosity of at least two orders of magnitude. Here, central properties correlate strongly with global rotation and shape: core galaxies tend to be boxy and slowly rotating, whereas power-law galaxies tend to be disk-like and rapidly rotating. A search for inner disks was conducted to test a claim in the literature, based on a smaller sample, that power laws originate from edge-on stellar disks. We find only limited evidence for such disks and believe that the difference between core and power-law profiles reflects a real difference in the spatial distribution of the luminous *spheroidal* component of the galaxy. The dense power-law centers of disk-like, rotating galaxies are consistent with their formation in gas-rich mergers. The parallel proposition, that cores are the by-products of gas-free stellar mergers, is less compelling for at least two reasons: (1) dissipationless hierarchical clustering does not appear to produce core profiles like those seen; (2) core galaxies accrete small, dense, gas-free galaxies at a rate sufficient to fill in their low-density cores if the satellites survived and sank to the center (whether the satellites survive is still an open question). An alternative model for core formation involves the orbital decay of massive black holes (BHs) that are accreted in mergers: the decaying BHs may heat and eject stars from the center, eroding a power law if any exists and scouring out a core. An average BH mass per spheroid of 0.002 times the stellar mass yields cores in fair agreement with observed cores and is consistent with the energetics of AGNs and the kinematic detection of BHs in nearby galaxies. An unresolved issue is why power-law galaxies also do not have cores if this process operates in all hot galaxies.

1. INTRODUCTION

The *Hubble Space Telescope* (HST) allows us to study the centers of nearby galaxies with a resolution of a few parsecs. The centers of galaxies are interesting for several reasons: (1) some galaxy centers harbor AGNs and QSOs; (2) many or most galaxy centers may contain massive black holes that are the remnants of dead QSOs; (3) dynamical processes such as relaxation are more rapid near galaxy centers than elsewhere in the galaxy; thus interesting dynamical phenomena are likely to occur first near the center; (4) galaxy centers are to galactic astronomy as middens are to archaeologists: centers are the bottoms of potential wells and debris such as gas and dense stellar systems settle there, providing a record of the past history of the galaxy.

The systematic properties of the centers of ellipticals and spiral bulges (hereafter “hot galaxies”) were described by Lauer (1983, 1985a) and Kormendy (1982a, 1984, 1985, 1987a,b). They detected inner regions in many galaxies where the slope of the surface-brightness profile flattens out, which they termed *cores*. They measured the size and surface brightness of these cores and demonstrated *central parameter relations* that linked core properties with one another and with global properties such as luminosity and effective radius. In particular, cores in brighter galaxies were larger and of lower density. The most recent version of the central parameter relations using ground-based data was presented by Kormendy and McClure (1993). A major goal of this paper is to revisit the central parameter relations using new *HST* data on 61 galaxies. We shall show that *HST* broadly supports the ground-based scaling relations but elaborates upon them in important ways.

Historically, the existence of cores in hot galaxies has been accepted as “normal” — probably because familiar dynamical models for galaxies such as the isothermal sphere and King models possess cores. In the absence of a central compact mass, it is plausible that all physical variables should vary smoothly near the origin and hence be expandable in a Taylor series with only even powers of r . In particular, the surface brightness may be written

$$I(r) = I_0 + I_1 r^2 + O(r^4), \quad (1)$$

where r is projected radius. Using the conventional definition of core radius, a galaxy satisfying Eq. (1) would exhibit a core of radius r_c such that $I(r_c) = \frac{1}{2}I(0)$. Tremaine (1997) suggests the term “analytic core” for systems with cores in which all physical variables vary smoothly. The cores of King models and the isothermal sphere are thus analytic, while the $R^{1/4}$ law is not.

HST observations show that real cores are not analytic. In analytic cores, the surface brightness flattens at small radii as $d \log I / d \log r \propto r^2$ — note that this is stronger than the usual condition for a flat profile, $d \log I / d \log r \rightarrow 0$ — whereas real cores show shallow power-law cusps into the resolution limit (Crane *et al.* 1993; Kormendy *et al.* 1994; Jaffe *et al.* 1994; Lauer *et al.* 1995, hereafter Paper I; Kormendy *et al.* 1996a). Fits in Byun *et al.* (1996, Paper II) yield projected slopes $\gamma \equiv -d \log I / d \log r$ in the range 0.05–0.3 for surface brightness, while non-parametric inversions for space density show even steeper slopes, from 0.2 to 1.1 (Gebhardt *et al.* 1996, Paper III; and Kormendy *et al.* 1996a). Thus, real cores have divergent rather than constant densities as $r \rightarrow 0$.

So far, cores have been found only in luminous ellipticals. The division between core and non-core galaxies is fairly sharp. Surface-brightness profiles either flatten out to form cores or continue to rise steeply into the resolution limit — few galaxies are in between (Kormendy *et al.* 1994; Jaffe *et al.* 1994; Paper I; Kormendy *et al.* 1996a). Statistical analysis of non-parametrically derived space density profiles indicates the existence of two groups (core and non-core) at the 90% confidence level (Paper III).

Paper I introduced the term *power laws* to describe the steeply rising, featureless profiles that lack cores.⁵ It is possible that the power-law category as we have drawn it may be oversimplified: At present the category contains a number of low-luminosity galaxies whose upper limits on core size are larger than those predicted by extrapolation of the core-luminosity relationship defined by brighter galaxies. In other words, some of the low-luminosity power-law galaxies may really be part of a core sequence extending to lower luminosity. Recent WFPC2 images in fact show tiny cores in a few power-law galaxies (Lauer *et al.* 1997). Nevertheless, the upper limits on core size for *brighter* power-law galaxies are already well below the core sequence for galaxies of similar luminosity, and thus clearly differentiate them. Future results may compel some revision of the power-law category, but the present simple core/power-law division is a useful working hypothesis.

Lauer (1985a) emphasized that the *central* properties of hot galaxies do not correlate perfectly with *total* luminosity and sought an explanation in terms of a second parameter. The present data suggest that this second parameter is related to global rotation and isophote shape. So far, cores have been found only in luminous, slowly rotating ellipticals with boxy isophotes⁶, while power laws are found in faint, rapidly rotating galaxies with disk isophotes. A link between central profile type and global shape/rotation was suggested by Nieto *et al.* (1991a) based on ground-based images, and further evidence was presented by Jaffe *et al.* (1994) and Ferrarese *et al.* (1994) based on *HST* images of 14 Virgo galaxies. The present database is considerably larger and permits a critical examination of this link and its relation to hot galaxy formation. Our point of view differs importantly from that of Jaffe *et al.*, who ascribe many of the differences between the two profile types to inclination effects connected with a small inner disk seen either face-on or edge-on. In contrast, we — like Nieto *et al.* — believe that the spheroidal light distributions are intrinsically different in the two types and would look the same from any viewing angle. These differences in viewpoint are discussed in Section 5 and Appendix A.

The results we have described raise several theoretical issues: why are there two types of profile and how did each type form? Why do the two types have different global rotation and shape? Why are cores non-analytic? And what do central profiles tell us about hot galaxy formation and evolution?

The second, more speculative, part of this paper addresses these issues. We suggest in Section 7 that the power-law profiles of disk galaxies indicate dissipation and are therefore consistent with formation in *gas-rich* mergers. The parallel suggestion — that the cores of

⁵ Cores and power laws were also identified by Jaffe *et al.* (1994), who called them Type I and Type II.

⁶ Isophote shape in elliptical galaxies is explained and defined by Bender & Möllenhoff (1987). A recent discussion is given by Kormendy & Bender (1996).

boxy galaxies are the by-products of *purely stellar, gas-poor* mergers — is more problematic. For example, luminous core galaxies are expected to accrete small dense satellites. The rate of such accretions appears sufficient to gradually fill in all low-density cores if such satellites survived and sank to the center. An unresolved issue is whether the satellites do survive, and thus whether some other process is needed to defend low-density cores against in-fill.

Even if the data do not firmly require such a mechanism, there is strong and growing evidence for a widespread population of massive central black holes (BHs) in hot galaxies (Kormendy & Richstone 1995). The presence of these objects must be taken into account in standard merger-based models for forming hot galaxies (Section 8). The BHs associated with the merging galaxies form binaries whose orbits then decay. The orbital decay heats the surrounding stars, erodes a power law if one exists, and scours out a core. Accreted satellites will also tend to be ripped apart, thus preventing core in-fill. BHs with plausible masses (as estimated in Appendix B) seem able to produce cores of roughly the right size and scaling versus galaxy luminosity. In this way, the presence of central BHs might “rescue” the dissipationless, gas-poor model for cores and boxy galaxies. However, models of core formation based purely on massive BHs leave several questions open, notably how power-law profiles escape similar disruption.

Whether or not these speculations about galaxy formation are correct, the updated relations between central and global galaxy parameters that are presented in this paper appear to provide important new constraints on hot galaxy formation.

2. CENTRAL PROFILE TYPES

Major collections of *HST* central profiles include Crane *et al.* (1993), Jaffe *et al.* (1994), Forbes *et al.* (1995), and Paper I. An assortment of representative surface-brightness profiles of 55 ellipticals and spiral bulges is given in Fig. 1. The following summary is based on the data and discussion in Paper I.

We distinguish two types of hot galaxy:

- (1) *Core galaxies* have “broken” power-law surface-brightness profiles that change slope significantly at a “break radius” r_b . To identify a galaxy as having a core, we require that the absolute value of the inner logarithmic slope, $\gamma \equiv -d \log I / d \log r$, be shallower than 0.3. Nearly all core galaxies appear to have $\gamma > 0$, which indicates a cusp in the central surface brightness and an even stronger cusp in the luminosity density. Paper III concluded that, even with errors taken into account, only 2 out of 15 known core galaxies could admit an analytic core ($\gamma = 0$). Core galaxies as a class are luminous objects with $M_V \lesssim -20.5$ ($H_0 = 80 \text{ km s}^{-1} \text{ Mpc}^{-1}$). They range from brightest cluster galaxies down to the intermediate-mass field elliptical NGC 3379.
- (2) *Power-law galaxies* show fairly steep surface-brightness profiles with no significant break within $10''$ (at Virgo). Their average surface-brightness slope is $\gamma \simeq 0.8 \pm 0.3$ at the smallest resolvable radius. Power-law galaxies are generally fainter than core galaxies ($M_V > -22$), but their luminosity densities at 10 pc are 10–1000 times higher than those of cores (Paper I). Profile shapes within $0''.1$ are generally not known,

though recent WFPC2 images suggest small cores inside some power laws. Power-law galaxies include M 32 (NGC 221), small Virgo ellipticals, and bulges of disk galaxies.

Both profile types are well fit by the following equation (the “Nuker” law, Papers I and II):

$$I(r) = I_b 2^{(\beta-\gamma)/\alpha} \left(\frac{r_b}{r}\right)^\gamma \left[1 + \left(\frac{r}{r_b}\right)^\alpha\right]^{(\gamma-\beta)/\alpha}. \quad (2)$$

The asymptotic logarithmic slope inside r_b is $-\gamma$, the asymptotic outer slope is $-\beta$, and the parameter α parameterizes the sharpness of the break. The break radius r_b is the point of maximum curvature in log-log coordinates. “Break surface brightness,” I_b , is the surface brightness at r_b . Equation (2) is intended to fit only over radii accessible to the HST Planetary Camera, i.e., $<10''$. For typical fitted values of β , there must be a further turndown in the profile at larger radii for the total luminosity to be finite.

Nuclei are identified when excess light above the prediction of Eq. (2) is visible within the inner few tenths of an arcsec. Nuclei with varying degrees of prominence are illustrated in Paper I (Fig. 14). Objects with prominent nuclei are always systems of low luminosity and are probably nucleated dSph or dE galaxies. Nuclei are assumed to be star clusters (or possibly unresolved tiny stellar disks), but direct spectral confirmation is often lacking. A stellar nucleus in NGC 3115 has been resolved in recent WFPC2 images (Kormendy *et al.* 1996b). Non-thermal central point sources exist in four galaxies in our sample: M 87 (NGC 4486), NGC 6166, Abell 2052 (Paper I) and NGC 4594 (Kormendy *et al.* 1996c). We call these *AGNs* to distinguish them from nuclei. So far, no nuclei (as opposed to AGNs) have been found within cores (Kormendy & Djorgovski 1989; Paper I).

Resolution plays an important role in classifying profiles and estimating central properties. This is illustrated in Fig. 2, which shows M 31 (NGC 224) and M 32 (NGC 221) as seen at their actual distances and as they would be seen 24 times further away just beyond Virgo (for future reference, we call these artificially positioned galaxies M 31-in-Virgo and M 32-in-Virgo). Up close, M 31 shows a two-component profile that is clearly divided into a bulge and a nucleus, the latter showing a small core. The entire profile shows too much substructure to fit comfortably into either the core or power-law category. In contrast, M 31-in-Virgo shows only a trace of a nucleus, and its profile and degree of nucleation are similar to those of several other galaxies that we have classed as power laws (see Fig. 14 in Paper I for a collection of power laws with varying degrees of nucleation). M 31 implies that many power-law galaxies, particularly those with hints of nuclei, may contain significant substructure, including nuclei and tiny cores.

M 32 is similarly ambiguous. Seen up close, M 32’s profile in Fig. 2 breaks from a power law near $0''.5$, curving gently downward into the resolution limit. M 32-in-Virgo shows a nearly perfect power law with only a small bend at the equivalent nearby radius of $70''$. Thus M 32 does not fit Eq. (2) very well either, because of multiple breaks that yield different values of r_b depending on what portion of the profile is fitted. M 32 shows that values of r_b in power-law galaxies are not robust and that similar breaks at small radii could exist in other distant power-law galaxies, even those that apparently show clean power laws at the present resolution.

Because the fitted values of r_b in power-law galaxies are less robust than those for core profiles, which reflect real features, we regard them as less fundamental. As explained below, we treat the fitted values of r_b differently in analyzing the two types of galaxy.

3. GALAXY SAMPLE AND DATABASE

The database used in this paper is contained in Tables 1, 2, and 3. A brief overview is given here, and additional details are provided in the table notes. The heart of the sample consists of 42 normal ellipticals and bulges taken from Paper I (NGC 4150, NGC 4826, and NGC 5322 were excluded due to strong nuclear dust). To these were added images of 14 E’s and bulges from the WFPC1 GTO programs (some unpublished). Five more normal E’s, mostly Virgo galaxies from Jaffe *et al.*, were located in the HST public archive as of June 1993, for a total of 61 galaxies. The original GO/GTO program and references to published *HST* profiles are listed in Table 1. All images were taken using the Planetary Camera in Cycles 1 and 2 and consequently suffer spherical aberration. They were observed through filter F555W, which approximates the V band, and usually have a peak signal of $\geq 10^4$ photons in the central pixel. All images were processed as described in Paper I and deconvolved with the same Lucy-Richardson procedure used there.

Power-law galaxies with identified nuclei are divided into two types: “moderately” and “severely” nucleated, indicated in Table 1 by “+” and “++”. M 31-in-Virgo is adopted as the dividing line between the two types (cf. Fig. 2 here and Fig. 14 of Paper I). In severely nucleated galaxies and in galaxies with AGNs, fits to the nuker law ignore the innermost pixels affected by the nuclear light.

Table 1 presents observed quantities such as Hubble type, distance, magnitude, color, and nuker-law parameters from Paper II. A few galaxies not treated in Paper II have been similarly fit and the results are given here. M 31 and M 32 appear twice, as seen nearby and near Virgo (labeled with a “V”). For core-type profiles, we accept the nuker-law fits as given for θ_b and μ_b .⁷ For power-law galaxies, no core is resolved, and we use the separate upper limits on core size and surface brightness provided by Paper I. These limits (for power laws only) are called θ_b^{lim} and μ_b^{lim} in Table 1. For a few power-law galaxies not contained in Paper I, these limits were obtained from a visual estimate of the steepness of the innermost part of the profile.

The distance to each galaxy (in km s^{-1}) has been estimated using a variety of methods as summarized in the notes to Table 1, and the adopted value and its conversion to Mpc (based on $H_0 = 80 \text{ km s}^{-1}\text{Mpc}^{-1}$) are given there. These distances are used to convert the apparent quantities in Table 1 to absolute quantities in Table 2. B-band magnitudes are converted to the V band to be consistent with the *HST* profiles. Data taken from the literature include central velocity dispersion, σ_0 , an inner velocity dispersion gradient defined as $R_\sigma \equiv \sigma_0/\sigma(10'')$, dimensionless rotation parameter $(v/\sigma)_*$, isophote shape a_4/a , global (effective) radius r_e , and global surface brightness μ_e , defined as the mean surface brightness *within* r_e . Details and sources are given in the notes.

⁷ The quantity θ_b is the break radius in arcsec, while μ_b is break surface brightness I_b expressed as V mag arcsec⁻².

Table 3 presents several derived quantities based on spherical, isotropic dynamical models fitted to the nuker-law light profile. The mass-to-light ratio of each model has been determined by normalizing to σ_0 from Table 1, assuming constant M/L with radius and equating σ_0 to the light-weighted rms line-of-sight dispersion in a centered $2''$ by $2''$ aperture (corrections for $1''$ FWHM seeing are at most a few percent and are not included). Mass-related quantities are blank if σ_0 is not available. Quantities tabulated at $0''.1$ include the luminosity density, peak Maxwellian phase-space density, two-body relaxation time, and predicted projected velocity dispersion. Total luminosity and mass within a sphere of the same radius are also given. Comparison to the non-parametric densities in Paper III indicates that nuker-law fitted luminosity densities are 10% too low on average but otherwise show little scatter for non- and moderately nucleated galaxies (severe nuclei were ignored in fitting nuker laws, and as a result nuker-law densities in these galaxies are about a factor of 2 lower than the non-parametric inversions). Several quantities are repeated for $r = 10$ pc, but for many galaxies this is well inside the resolution limit of $0''.1$ and requires an inward extrapolation of the nuker-law fit.

An impression of the division into core and power-law galaxies is provided by Fig. 3, which plots inner power-law slope γ versus observed break radius θ_b (or θ_b^{lim} for power-law galaxies) in arcsec. Profiles with $\theta_b \geq 0''.16$ ($\log \theta_b \geq -0.8$) are reasonably well resolved by *HST*. They divide into two groups, those with $\gamma \leq 0.25$ (cores) and those with $\gamma > 0.5$ (power laws) — the valley in between is empty. This is the division that motivated the two profile types in Paper I, later analyzed statistically in Paper III.

The rectangular box in Fig. 3 encloses galaxies that we are fairly sure contain real cores. Galaxies above the box are definitely power laws at current resolution. Galaxies to the left of the box are classed as power laws although some contain a hint of an incipient core. The effect of limited resolution is apparent for M 31 and M 32; both galaxies are plotted twice, as seen nearby and at Virgo. The plotted positions differ appreciably, reflecting features of their inner profiles that cannot be probed in more distant galaxies.

Galaxies within the box in Fig. 3 comprise the “Core” sample used in the following section. All others are classed as power laws.

4. CENTRAL PARAMETER RELATIONS

The data in Tables 1 and 2 are used to plot new central parameter diagrams like those of Lauer (1983, 1985a) and Kormendy (1985, 1987a,b). We begin with plots versus absolute magnitude in Figs. 4a,b,c,d. The symbols have the following meanings:

- (1) Core galaxies are plotted with filled circles (\bullet) using values of r_b and μ_b from Table 2.
- (2) Power laws are plotted with open circles (\circ) using the limits r_b^{lim} and μ_b^{lim} from Table 2.
- (3) M 31 and M 32 are plotted twice, as seen at their actual distance (asterisks) and in Virgo (end of vector). The length and direction of these vectors illustrate the possible effect of changing resolution on other power-law galaxies. Their direction is opposite to the limit flags that are attached to all power-law galaxies.

- (4) Special objects: The S0 galaxy NGC 524 is the only core profile that is found within a bulge (all others are in ellipticals). NGC 524 is roughly face-on and shows flocculent dusty disk arms (Paper I) and a blue center (Kormendy, private communication); it is plotted with a small square. Fornax A (NGC 1316) is a probable recent merger remnant (Schweizer 1980) with a peculiar morphology (RC3). It has an abnormally small core for a galaxy of its luminosity (Kormendy 1987b). NGC 4486B shows a double nucleus like M 31's in WFPC2 images (Lauer *et al.* 1996) but continues to have a clearly defined core.

The new plots show the same broad trends versus galaxy luminosity that were seen in ground-based data (Kormendy & McClure 1993). Core galaxies are luminous objects that extend down to $M_V = -20.5$. All normal ellipticals brighter than $M_V = -22$ show cores, with cores of brighter galaxies being larger and lower in surface brightness and density. The new central parameters of core galaxies correlate well with previous values measured from the ground (Kormendy *et al.* 1994). The parameter relations for core galaxies are fairly narrow; for example, the rms scatter in r_b versus M_V about the best-fitting line is only 0.25 dex (Fornax A omitted).

Ferrarese *et al.* (1994) have questioned whether the trends in core properties versus absolute magnitude are an artifact created by adding brightest cluster galaxies (BCGs) to smaller, trendless galaxies. They argue that, aside from M 87, all cores in their Virgo sample are of similar size, and trends appear only when M 87 is added. Although M 87 does not strictly qualify as a BCG (that distinction in Virgo is held by NGC 4472), it does share certain properties with BCGs such as high luminosity and central location within a subcluster.

From our larger sample, it seems clear that trends in core properties versus M_V are real and are not an artifact of adding BCGs. The present sample could be truncated at $M_V = -22.2$ to eliminate *all* BCGs (including those in small groups as well as Abell clusters), yet trends among the 11 remaining core galaxies between $M_V = -20.5$ and -22 would still be present. In all plots, core properties of BCG galaxies appear to be a normal extension of the cores in smaller core ellipticals.

Power-law galaxies in Fig. 4 are low-to-intermediate luminosity systems that extend in luminosity up to $M_V = -22$. They overlap with core galaxies at intermediate magnitudes in the range $-20.5 > M_V > -22$. Despite an increase in angular resolution by a factor of 10 with *HST*, we have generally failed to find cores in these objects, and thus their distribution in Fig. 4a is rather flat, reflecting the constant *HST* resolution limit of ~ 0.1 arcsec. For systems fainter than $M_V \approx -19$, this limit is uninteresting since it equals or exceeds predictions based on extrapolation from core galaxies. However, at intermediate magnitudes in the range $M_V = -20.5$ to -22 , power-law and core galaxies coexist, and it is clear that the *scatter* in break radius is real and large. Core/power-law pairs that illustrate extremes of r_b at fixed luminosity include NGC 3379 and NGC 1023, whose break radii differ by more than a factor of 40 while their absolute magnitudes differ by less than 0.5 mag, and NGC 4168 and NGC 4594, for which the ratio of break radii is over 100 even though their absolute magnitudes are almost identical. This is not a resolution effect wherein cores are detected in nearby galaxies but not in distant ones. Figure 5 plots break radius versus distance and shows that most of the sample, containing both small and large

cores, resides in a narrow range of distance near that of Virgo. More distant galaxies are actually *more* likely to show cores because their cores are intrinsically larger.

The large scatter in break radii near $M_V = -20.5$ to -22 might at first sight be taken as a manifestation of the two-dimensional, planar distribution of the global structural parameters of hot galaxies, i.e., the *fundamental plane* (Dressler *et al.* 1987; Djorgovski & Davis 1987; Faber *et al.* 1987). Two-coordinate projections of this two-dimensional distribution commonly exhibit scatter depending on whether they show the plane edge-on or face-on. The basic coordinates for the global plane (see Section 6) are r_e , μ_e , and σ_0 , from which L_V can be derived as $L_V = 2\pi\mu_e r_e^2$. A plot of radius versus magnitude is thus a projection of the fundamental plane, and scatter might be expected in r_b versus M_V that is comparable to that seen in r_e versus M_V , provided r_b and r_e are well correlated.

This hypothesis is tested by substituting r_e for r_b in Fig. 4d. The scatter there proves to be small, demonstrating that the combination of radius versus L shows the *global* plane rather close to edge-on. The much larger scatter of Fig. 4a therefore suggests a *real decoupling* of central properties from global ones, as emphasized by Lauer (1985a). In Section 5 we examine this scatter in more detail and show that it correlates with global rotation and isophote shape, in the sense that power-law galaxies (which have small r_b) are disk-like and rotate rapidly, while cores (which have large r_b) are boxy and rotate slowly.

Bulges are distributed in Fig. 4 like ellipticals of small-to-intermediate size. None (except for M 31-nearby) shows a core. The resemblance of bulges to small and intermediate ellipticals is not surprising since the two classes of galaxy share several traits, including similar global size, high rotation, flattening by rotation rather than anisotropy, and disk-like subsystems (Bender, Burstein & Faber 1992).

Before drawing further conclusions from Fig. 4, we consider whether the trends shown there are affected by the particular sample of galaxies chosen. The present sample is a mixture taken from different authors, but we have been careful to retain only objects that are *morphologically normal* and *free of dust*. Our own sample from Paper I (comprising 42 out of the 61 total objects in this paper) was specifically chosen to probe the full range of parameters covered by the ground-based central parameter relations (Lauer 1985a; Kormendy & McClure 1993). We strove hard to sample the widest possible magnitude range and, at intermediate magnitudes, to sample galaxies with both large and small apparent cores. Thus, it is possible that the present sample somewhat exaggerates the total spread in break radii at middle magnitudes.

Another point is that most objects studied here had previous ground-based data, and thus some prior clue as to core size. Since ground data typically agree well with *HST* data (especially for large galaxies, Kormendy *et al.* 1994), the present sample does not provide a truly fresh look at galaxy centers. A sample to do this with completely new galaxies has been observed in Cycle 5 and is now being analyzed. What the present sample does is fairly probe galaxies that had previously been examined from the ground.

Are the claimed correlations robust for core galaxies specifically? Although Fornax A has been included in the diagrams for interest, it is strongly peculiar and its center is contaminated by dust (Shaya *et al.* 1996). It does not qualify for our sample of normal, massive E's, and its high residuals should not count against the correlations. Six more core ellipticals with ground-based data could also be added to bolster the *HST* data; these

new galaxies agree well with the trends here (Kormendy, unpublished). Thus we feel that evidence strongly favors the core correlations found in Fig. 4; however, full confirmation will require the completely independent sample of galaxies from Cycle 5 that we are now analyzing.

Finally, the number of galaxies at intermediate magnitudes is still small. We will argue in the next section that the spread of properties in this magnitude range is correlated with global boxiness and diskiness, and will draw from this some significant conclusions about hot galaxy formation. Clearly, these conclusions will need to be checked by gathering a larger and more representative sample of galaxies at these magnitudes. Again, the Cycle 5 sample was selected to do this.

The referee has asked whether bright power-law galaxies might in fact all be S0's (or bulges). There are 7 power-law galaxies in the magnitude range -20.5 to -22 : NGC 596 (E⁺4:), NGC 1172 (E⁺2:), NGC 1700 (E4), NGC 3115 (S0⁻), NGC 4594 (Sa), NGC 4621 (E5), and NGC 4697 (E6) (Hubble types from the RC3). Two of these are actual disk galaxies (NGC 3115, NGC 4594), two more are highly flattened E's (NGC 4621, NGC 4697), and two more have S0-like outer envelopes (NGC 596, NGC 1172). That leaves only NGC 1700, which is also fairly flattened. We will show in the next section that there is a good correlation between power-law galaxies and galaxies that are rapidly rotating with disk-like isophotes. Thus it is possible that all bright E-type power-laws are in fact S0's masquerading as ellipticals.

It is interesting to speculate where the bright power-law galaxies will move within Fig. 4 as resolution improves. At present these galaxies fall below the core sequence by $\times 3$ - 10 in core size. However, new WFPC2 observations have increased this distance for a number of them (Lauer *et al.* 1997). It is thus possible that bright power-law galaxies may ultimately emerge as a separate population rather than simply tracing the lower edge of a large dispersion in core size at these luminosities.

M 31 and M 32 again show the effect of changing spatial resolution. M 32-in-Virgo lies near the Virgo dwarf E's in all of its parameters, suggesting that the downward trend in surface brightness for faint galaxies in Fig. 4c is mainly an artifact of resolution. M 31-in-Virgo is indistinguishable from other bulges of similar magnitude. Its shift in the diagrams under distance change is not as large as that of M 32 because its profile is not as steep as M 32's between $0''.1$ and $2''.4$ (Fig. 2).

NGC 4486B is the lone core galaxy near $M_V = -17.5$ mag. Its angular size lies near the lower boundary of established cores in Fig. 3, but the presence of a core has been confirmed in WFPC2 images (Lauer *et al.* 1996). NGC 4486B's low luminosity, compact profile, high line-strength, and close proximity to M 87 suggest that it might be tidally stripped by its larger neighbor (Faber 1973). Its core parameters would be consistent if it once resembled the small-core galaxy NGC 3608 and then lost $\sim 90\%$ of its outer luminous envelope. Whether a core could actually survive such extensive stripping and whether a diffuse giant like M 87 could strip a high-density object like NGC 4486B are open questions (see Section 7.3.2).

Figure 6 plots luminosity density, mass density, and phase-space density at a limiting radius of $0''.1$ (from Table 3) as a function of absolute magnitude. An impressive feature of Fig. 6 is the large range in density from small to large galaxies, almost 10^6 in all three

panels; half of this range is spanned by cores alone. Part of this spread is due to the fact that Fig. 6 mixes objects at different distances. However, densities at the fixed physical scale of 10 pc still show a range of 1000 (column 13, Table 3; see also Fig. 13, Paper I; note that densities in distant galaxies at 10 pc require inward extrapolation). The large range of densities near the centers of hot galaxies has been remarked on before (Kormendy 1984, Lauer 1985a, Carlberg 1986), but *HST*'s higher resolution has pushed up densities in power-law galaxies by another two orders of magnitude. As discussed in Section 7, the large density contrast between small and large hot galaxies is an important clue to hot galaxy formation.

We conclude this section by presenting general scaling laws for core properties versus galaxy luminosity and mass. We restrict attention to core galaxies because their parameters are robust. It is well known (see Section 6) that cores are really a *two-dimensional* dynamical family (the fundamental plane). Nevertheless, it is often convenient to treat them as a one-parameter family depending on luminosity or mass. This is possible because (1) the fundamental plane is only partially filled, and projections against any pair of coordinate axes have only limited extent; (2) typically, these projections are elongated and can be approximated by one-dimensional scaling relations; and (3) core mass and luminosity are both moderately well related to global mass and luminosity for core galaxies. This combination produces the tight correlations versus total luminosity in Figs. 4 and 6, which we now quantify.

The following is a set of self-consistent scaling relations versus L_V and galaxy mass, M . Total luminosity has been related to mass by assuming $(M/L_V) \propto L_V^{0.25}$ (Faber *et al.* 1987). The exponents in these relations are not least-square fits but have been derived by a process of trial-and-error adjustment to maintain consistency with standard structural formulae. The first three of these relations are independent fits to the data, while the rest are derived from the structural formulae. The relations involving M_{core} assume that the core is in dynamical equilibrium.

$$r_b \propto L_V^{1.15} \propto M^{0.92}, \quad (3)$$

$$I_b \propto L_V^{-1.0} \propto M^{-0.8}, \quad (4)$$

$$\sigma_0 \propto L_V^{0.2} \propto M^{0.16}, \quad (5)$$

$$j_{core} \sim \frac{I_b}{r_b} \propto L_V^{-2.15} \propto M^{-1.72}, \quad (6)$$

$$L_{core} \sim I_b r_b^2 \propto L_V^{1.3} \propto M^{1.04}, \quad (7)$$

$$M_{core} \sim \sigma_0^2 r_b \propto L_V^{1.55} \propto M^{1.24}, \quad (8)$$

$$M_{core}/L_{core} \sim \frac{\sigma_0^2}{I_b r_b} \propto L_V^{0.25} \propto M^{0.2}, \quad (9)$$

$$\rho_{core} \sim \frac{\sigma_0^2}{r_b^2} \propto L_V^{-1.9} \propto M^{-1.52}. \quad (10)$$

5. SCATTER IN THE CENTRAL PARAMETER RELATIONS: CORRELATIONS WITH GLOBAL ROTATION AND ISOPHOTE SHAPE

An emerging suspicion of the last decade is that there are actually *two* types of elliptical galaxies: luminous E's with boxy isophotes that rotate slowly, and small E's with disk-like isophotes that rotate rapidly (Bender 1988; Nieto 1988; Nieto & Bender 1989; Bender *et al.* 1989; Kormendy & Djorgovski 1989). A formal division of the Hubble sequence for ellipticals into two classes has been suggested based on these criteria (Kormendy & Bender 1996). We shall refer to these two subtypes as *boxy* and *disky* respectively.

The scatter seen in central parameters versus absolute magnitude in Figs. 4 and 6 appears to correlate with boxy/disky subtype. This correlation is illustrated in Fig. 7, which replots Fig. 4a (r_b versus M_V) but now with symbols indicating rotation, $(v/\sigma)_*$, in Fig. 7a, and isophote shape, a_4/a , in Fig. 7b. It is seen that power-law galaxies are mainly rapidly rotating and disk-like, while cores are slowly rotating and boxy or neutral. *At intermediate magnitudes, $M_V = -20.5$ to -22 , the presence of a core is a better predictor of boxiness or slow rotation than is absolute magnitude.* The same correlation was also found by Nieto *et al.* (1991a) using ground-based data. In our sample, the correlation between disk-like galaxies and power laws appears strongest if the disk-like threshold is set at $a_4/a \geq 0.4$. All other isophote types (boxy, neutral, and variable) are associated with cores. "Variable" galaxies are those with strongly varying values of a_4/a versus radius. We use the term *boxy* to include the boxy, neutral, and variable types.

Jaffe *et al.* (1994) and Ferrarese *et al.* (1994) also saw a link between power-laws and disks based on their *HST* Virgo sample. They went further to suggest that essentially all power laws have *inner* disks within $1''$ and that such disks seen edge-on are what produce power-law profiles (Jaffe *et al.* 1994). We agree that power laws tend to reside in galaxies with *globally* high rotation and global diskiness, but we do not see evidence for *inner* disks in all or even most power laws. Rather, we believe that the *hot* component is intrinsically different in cores and power laws and that the two classes therefore would look different from any viewing angle.

This difference in interpretation is fundamental, since implications for galaxy formation would be limited if profiles were a sensitive function of viewing angle. We believe that Jaffe *et al.* were influenced by the fact that most power-law objects in their sample happened to be highly flattened, edge-on, late-type E/S0's with a higher-than-average incidence of both inner and outer disks. Our power-law galaxies as a group are less flattened, less edge-on, less skewed to late Hubble types, and do not in general show inner *or* outer disks. A brief discussion of the edge-on disk model for power laws was presented in Paper I. A more extensive search for inner disks was made with the present larger sample, and the results are reported in Appendix A.

To summarize, it appears likely that disk-like and boxy ellipticals have different kinds of central light profiles. Since *global* properties are implicated, whatever process established this connection was probably a major event in the life of the galaxy. We explore this link and its implications for hot galaxy formation in Section 7.

6. THE CORE FUNDAMENTAL PLANE

So far we have focussed on the relationship between the centers of galaxies and their global properties. We turn next to relationships among the central properties alone. Plotting galaxies in central $(\log r_b, \mu_b, \log \sigma_0)$ -space allows us to look for a fundamental plane (FP) analogous to the one found in global $(\log r_e, \mu_e, \log \sigma_e)$ -space (Dressler *et al.* 1987; Djorgovski & Davis 1987; Faber *et al.* 1987). If cores are in dynamical equilibrium (highly likely), if they are supported by random motions (as indicated by the observations), if velocity anisotropy does not vary too much from galaxy to galaxy (unknown, but see below), and if core M/L is a well-behaved function of any two variables μ_b , r_b , or σ_0 (true of global M/L), then we expect cores to populate a thin surface in central $(\log r_b, \mu_b, \log \sigma_0)$ -space (Faber *et al.* 1987). Lauer (1985a) demonstrated that cores of well-resolved galaxies indeed populate a two-dimensional manifold, and Faber *et al.* (1987), using Lauer’s data, derived a preliminary core fundamental plane that was roughly parallel to the global FP. We revisit the tilt and thickness of this plane using the more accurate *HST* data.

Figure 8 shows projections of $(\log r_b, \mu_b, \log \sigma_0)$ -space for the present sample. Cores are again filled circles, while power-law galaxies (open circles) have been plotted for completeness’ sake using their limiting values (warning: the direction of the limit flags is schematic using M 31 and M 32 as a guide). To seek a plane, we rotate about an axis and search for the thinnest distribution of points. Following Faber *et al.* (1987), we choose to rotate about the σ_0 -axis because the resulting combination of I_b and r_b is nearly invariant to small resolution changes and small measurement errors. The best rotation (based on core galaxies only) is shown in Fig. 8d. Within the errors, the tilt of this FP is consistent with the global plane, $\sigma^{1.35} \sim r_e I_e^{0.84}$, found by Faber *et al.* (1987); this is the orientation plotted. The residual rms scatter about this plane, expressed as an error in $\log r_b$, is 0.12 dex (for cores only). This is 30% larger than the equivalent scatter about the global FP, which is 0.09 dex (Lynden-Bell *et al.* 1988). The larger scatter about the core plane may be related to the presence of central BHs, which elevate σ_0 in some galaxies. Five labeled objects with positive residuals in Fig. 8d are BH candidates from Kormendy & Richstone (1995) and Kormendy *et al.* (1996b,c).

The locus of I_b versus r_b is also quite narrow for cores (Fig. 8c). This occurs because the individual brightness profiles of core galaxies are approximately tangent to a single line in the $(\log r_b, \log I_b)$ plane, as can be seen in Fig. 1. This tight correlation can be used to construct a second distance indicator based on r_b and I_b alone. The scatter about the best-fitting line corresponds to 0.18 dex in log distance, which is two times worse than the global FP. However, the method does not require any measurement of σ and thus may sometimes be useful.

The existence of a core fundamental plane suggests that (1) cores are in dynamical equilibrium supported by random motions; (2) that r_b and I_b are meaningful dynamical parameters describing the size and luminosity density of the core; (3) that velocity anisotropy does not vary greatly among core galaxies; (4) that the mass of any central BH does not strongly dominate the core potential in most galaxies; and (5) that core mass-to-light ratio varies smoothly over the fundamental plane.

The core fundamental plane is well defined even though (1) the profiles of core galaxies are *not* analytic; (2) the profiles of different core galaxies are not identical (α and γ vary, Paper I); (3) the velocity dispersion anisotropy may vary from galaxy to galaxy; (4) some or all core galaxies may harbor massive BHs that distort both the photometric profile and σ_0 ; and (5) cores represent only a tiny fraction of the total luminosity of the galaxy. Evidently whatever differences exist among core galaxies are not so large as to erase the appearance of a two-parameter family of self-gravitating cores that is fundamentally not too dissimilar from the 2-dimensional family of isothermal spheres.

7. CENTRAL PARAMETER RELATIONS AND HOT GALAXY FORMATION

The final sections of this paper discuss the central parameter relations in the context of galaxy formation. We assume throughout that hot galaxies form via hierarchical clustering and merging (hereafter HCM; see e.g., Toomre 1977, White & Rees 1978, and Blumenthal *et al.* 1984). Descriptions of HCM as applied to hot galaxies may be found in Schweizer (1986), Kormendy & Sanders (1992), de Zeeuw & Franx (1991), Barnes & Hernquist (1992), and Bender *et al.* (1992). An important challenge to HCM is the formation of boxy and disk galaxies, including the association found here with central cores and power laws. A novel element that needs to be considered is the presence of massive BHs in the centers of many or most hot galaxies, which could considerably alter the predictions of standard HCM with no BHs.

We will suggest that the high-density cusps of power-law galaxies are broadly consistent with the growing body of evidence that points to the importance of *gaseous dissipation* in their formation. More of a puzzle are the low-density cores of massive hot galaxies — they seem hard to form in the first place and hard to maintain once formed. The problem of cores leads us to consider an alternative method for forming them based on central BHs. This model is the subject of Section 8.

7.1 Previous Work on Hot Centers

Many authors have discussed the centers of hot galaxies in the context of galaxy formation. Larson (1974a,b) computed gaseous collapse models for ellipticals and noted that central star formation could continue until very late, fueled by dregs of gas falling into the center. He conjectured that central star density might depend on a delicate balance between the dissipation rate, global star formation efficiency, and mass loss via supernova-driven winds.

Lauer (1983, 1985a) discussed the systematic properties of the centers of hot galaxies in light of new data. The high-density centers of small galaxies were consistent with Larson’s gaseous infall picture, but the same theory predicted greater gas retention, and hence denser centers, in the deeper potential wells of bright galaxies, contrary to observations. An alternative scenario based on dissipationless merging also ran into difficulties because N-body simulations showed denser cores forming as galaxies successively merged (Farouki *et al.* 1983); this “departure from homology” has been confirmed with more modern N-body simulations (Barnes 1992; Makino & Ebisuzaki 1996).

Carlberg (1986, see also Ostriker 1980) used phase-space density arguments to constrain the progenitors of hot galaxies. He noted that the high phase-space densities of small galaxies precluded their formation from *purely stellar* spiral disks because the phase-space density of spiral disks is low and phase-space density in dissipationless mergers remains constant or declines (Barnes 1992). However, HCM naturally incorporates gaseous merging as well as stellar merging (Schweizer 1986; Kormendy 1989; Kormendy & Sanders 1992), either during the main merger event (Negroponte & White 1983; Barnes & Hernquist 1991; Hernquist & Barnes 1991), during an earlier phase in which the disk progenitors develop bulges (Barnes 1992; Hernquist 1993), or during later gaseous infall. Thus it is no problem to create the high densities of small hot galaxies provided gaseous dissipation is present at some stage.

The above papers considered mainly equal-mass mergers, but small satellites can also be accreted by dynamical friction (e.g., Tremaine 1976). Kormendy (1984) applied this concept to the capture of small, dense ellipticals by larger ones (see also Balcells & Quinn 1990) and predicted the photometric and kinematic signatures of such events: cores-within-cores, high surface-brightness centers, central velocity dispersion dips, central counter-rotation, and isophote twists. Many of these anomalies have since been found (de Zeeuw & Franx 1991; Barnes & Hernquist 1992), leading to the concept of (photometrically and/or kinematically) *decoupled centers*. Altogether, roughly a third of hot galaxies show such anomalies (de Zeeuw & Franx 1991), with core galaxies showing them roughly twice as often as power laws (Nieto *et al.* 1991b, Paper I).

Hernquist & Barnes (1991) suggested an alternative way to make decoupled centers involving gaseous accretion and subsequent star formation in a cold inner disk. Decoupled subsystems are often dynamically colder than expected from purely stellar satellite accretion (Bender & Surma 1995, Franx & Illingworth 1988). Their stars are also stronger-lined than stars at the centers of small satellites, suggesting that local nucleosynthetic enrichment (and hence star formation) has taken place (Bender & Surma, 1988).

To summarize, the consensus exists that gaseous dissipation plus *in situ* star formation are the key factors responsible for the high central densities of small hot galaxies. Both cores and power-laws probably also contain both stellar and gaseous material captured in accretions and mergers. Less clear is why central properties scale at all with galaxy mass and in particular why the centers of massive hot galaxies are so diffuse.

7.2 Power Laws in Disky Galaxies

We turn now to the relation between central and global properties. The basic question is whether the core/power-law distinction found for the inner parts is consistent with theories for forming the outer parts.

The situation seems clearest for disk galaxies. The formation of disk hot galaxies, though not fully understood within HCM (Kormendy & Bender 1996), probably stems from the presence of significant quantities of *gas* during the latest merger(s). Several authors have noted that the high rotation, disk isophotes, and lack of minor-axis rotation of disk ellipticals imply global gaseous dissipation (Kormendy 1989; Nieto *et al.* 1991a; Bender *et al.* 1992). Recent simulations with gas (Barnes 1996, Barnes & Hernquist 1996)

show that just a few percent of the mass in gas is sufficient to destroy box orbits and impart high global rotation; the same gas can make disk isophotes if it forms stars.

The steep central power laws of disk galaxies are plausible by-products of such gaseous mergers. Numerical models of gas-rich mergers (Barnes & Hernquist 1991, Hernquist & Barnes 1991, Mihos & Hernquist 1994) have shown that angular-momentum transfer and dissipation can swiftly carry much of the gas in merging galaxies to the center of the remnant. Strong evidence for efficient gaseous infall is seen in nearby gas-rich merger remnants, which possess massive central clouds of gas (Sanders *et al.* 1988, Scoville *et al.* 1991) that may be fueling central starbursts (Bushouse 1987; Kennicutt *et al.* 1987; Leech *et al.* 1989; Condon *et al.* 1991; Solomon, Downes & Radford 1992; Kormendy & Sanders 1992). A major uncertainty is exactly where and how the stars form, and hence the shape and density of the resulting stellar profile; if anything, current models of starburst cusps are *too* dense and compact (Mihos & Hernquist 1994). This problem aside, the high-density cusps of power-law galaxies seem broadly consistent with their formation in dissipative, gas-rich mergers⁸.

7.3 Cores and Boxy Hot Galaxies

The above discussion supports the notion that disk galaxies and their central power-laws were formed together in gas-rich mergers. Analogous arguments suggest that boxy galaxies formed in gas-poor mergers (Binney & Petrou 1985; Bender & Möllenhoff 1987; Nieto 1988; Nieto & Bender 1989; Nieto *et al.* 1991a; Bender *et al.* 1992). The distinctive shape, slow rotation, anisotropy, and minor-axis rotation of boxy galaxies are consistent with a large population of stars moving on box orbits in a triaxial potential created during a dissipationless merger (Barnes 1988, 1992).

We therefore ask: are the core profiles of boxy galaxies simply the natural by-product of dissipationless stellar merging? To address this, the merging history of boxy galaxies can be simplified into two parts: an early phase in which centers originally formed, and a later phase involving the accretion of small satellite companions. Do core profiles form early, and do they survive later accretion?

7.3.1 Early Formation

The early formation of boxy, core galaxies is murky because their progenitors are poorly known⁹. Existing N -body simulations of dissipationless equal-mass mergers do not

⁸ It may be significant that 6 out of 7 power-law galaxies in our sample with $-20.5 > M_V > -22$ are *field* objects, whereas 6 out of 9 core galaxies in the same range are in *clusters*. Kauffmann (1996), using Press-Schechter theory, has proposed that the clustering history of intermediate-magnitude ellipticals depends on environment — those in clusters are old, while many in the field are formed from recent mergers of gas-rich spirals. A preponderance of power-laws in field galaxies would be consistent with their formation in recent gas-rich mergers. In fact, two of the 6 field power-law galaxies are known merger remnants (NGC 596 and NGC 1700; Schweizer *et al.* 1990).

⁹ It is clear, however, that bright ellipticals were *not* formed by simply merging *today's* faint ellipticals. This is precluded by their very different stellar populations (Bender *et al.* 1992) — each type must have had its own progenitors.

develop cores — rather, pre-existing cores tend to shrink slightly due to non-homology, and the central density increases at each level of merging (Farouki *et al.* 1983; Barnes 1992; Makino & Ebisuzaki 1996). Thus it appears that cores in luminous galaxies do not arise spontaneously in equal-mass merging, although the resolution of present N-body experiments is limited.

The problem may be worse with *unequal*-mass mergers, in which a smaller, denser component could sink to the middle, perpetuating a high-density center. This situation is discussed further under satellite accretion. On the other hand, progenitors of boxy galaxies may differ from today’s hot galaxies and may not obey the same inverse correlation between mass and density.

An entirely different way to generate low-density cores via stellar merging is to start with pure spiral disks. However, conventional density fluctuation spectra do not form spirals in the overdense environments that give rise to elliptical galaxies (Blumenthal *et al.* 1984, Bardeen *et al.* 1986). Yet a third way to make diffuse cores is via mass loss in stellar or AGN-driven winds, but the deeper potentials of luminous core galaxies should retain more gas, not less (Larson 1974b). A final possibility is to whip phase-space vacuum into centers during merging, for example via mergers of multiple subclumps (Weil & Hernquist 1996); however, it appears that the merging of the subclumps must be nearly simultaneous, which would be difficult to orchestrate for every core galaxy.

7.3.2 Late Satellite Accretion

The possible difficulty of forming cores may be matched or superseded by the even greater problem of maintaining them against satellite infall. In any merging hierarchy, the more luminous galaxies cannibalize the less luminous ones. It is plausible that the central region of the smaller galaxy will survive intact so long as its radius is smaller than the tidal radius imposed by the larger galaxy; this in turn implies that the regions of the smaller galaxy that are denser than the core of the large galaxy should survive.

In fact, the centers of today’s satellite galaxies are *much* denser than the centers of core galaxies (see Fig. 13, Paper I); typical power-law galaxies in the range $M_V = -17.5$ to -22 are 100 to 1000 times denser at 10 pc than Abell brightest cluster galaxies (BCGs), and are 3 to 30 times denser at 100 pc, the inner boundary where accreted satellites can be detected by *HST*. The tidal argument therefore suggests that dense satellites should survive infall, filling in low-density cores of bright galaxies as proposed by Kormendy (1984). Yet every bright galaxy in our sample (except Fornax A) has a low-density core.

To quantify this paradox, we estimate a typical satellite accretion rate for Abell BCGs. From counts of nearby companions and other data, Lauer (1988) deduced an accretion rate for BCGs of $0.2L^*$ per Gyr, in close agreement with a theoretical estimate by Merritt (1985). There are 7 Abell BCGs in the current *HST* sample, all of which have large, low-density cores.¹⁰ If satellite profiles are preserved during infall, accreted satellites over a particular magnitude range will be detectable. Small satellites have too little light, while large ones have profiles that are too similar to the BCG to make a difference. The profiles

¹⁰ They are NGC 2832, NGC 4889, NGC 6166, NGC 7768, Abell 1020, Abell 1861, and Abell 2052.

in Fig. 1 imply ¹¹ that satellites with M_V between -19.0 and -22.0 would be detectable in all 7 BCGs, and that those between -17.5 and -22.0 would be detectable in all but Abell 2052. If BCGs have been accreting for 5 Gyr at the rate estimated by Lauer (1988), this translates to 2 detectable accreted satellites per BCG, or 13 total accretions in 7 galaxies.

This estimate is conservative — gaseous accretion has been neglected, and the current accretion rate by BCGs is probably lower than average owing to the rise in cluster velocity dispersions with time. Restriction to Abell BCGs has excluded such near-BCGs as NGC 4874 in Coma (which was probably once the BCG of its subgroup), Virgo’s BCG, and BCGs of smaller groups like Pegasus, Fornax, and Eridanus (where accretion is probably faster owing to smaller velocity dispersions). Including such objects would double the number of primaries to 14 and raise the number of expected accretions to 26. However, no filled-in cores are seen in any of these BCGs.

So far we have assumed that the inner portions of accreted satellites survive while sinking to the centers of their primaries, based on the tidal disruption argument. This argument has been criticized by Weinberg (1994, 1997), who stresses that the time-dependent tidal force from the host galaxy can do work on resonant stars in a satellite galaxy even when the satellite is much denser than the host. Using semi-analytic perturbation theory and King-model profiles, Weinberg concludes that, if satellite and primary obey the global fundamental scaling law of Eq. (10), the satellite will be disrupted during its orbital decay if its mass exceeds 10^{-3} – 10^{-2} of the primary mass. If this were true, low-density cores would remain unaffected by late accretion because of satellite disruption.

The most relevant N-body simulation so far of satellite survival is a merger of two pure ellipticals with mass ratio 10:1 by Balcells & Quinn (1990). The density scaling of the small galaxy relative to the larger one approximately follows Eq. (10). At the end of the merger, the pre-existing core of the primary is filled in by an amount that would be detectable by *HST*. Further N-body models are in progress to check Weinberg’s analytic results (Dubinski 1997) and to simulate the dense central power-laws of real satellite galaxies (Minske & Richstone 1997). Realistic modeling of these dense centers may prove crucial.

To summarize this section, the link between the centers of hot galaxies and their outer parts must be accounted for in the HCM picture. Many properties of both disk and boxy galaxies are naturally explained by appealing to a difference in the amount of gas present during the most recent merger(s). Disk galaxies, including their high central densities, suggest final mergers that were *gas-rich*. Analogous arguments concerning boxy galaxies are less clear: the global kinematics of these galaxies suggest final mergers that were *gas-poor*, but forming and preserving cores in such models may be difficult. An enlargement of the HCM model for core formation that includes BHs is considered in the next section.

8. CORE CREATION BY MASSIVE CENTRAL BLACK HOLES

¹¹ Our criterion is that the net profile after infall be one magnitude brighter than presently observed at the inner resolution limit. This is sufficient either to erase a core in marginally resolved galaxies or create a tell-tale inner upturn in well-resolved cores.

High-resolution kinematic observations of galaxy centers strongly indicate that massive BHs are normal constituents of the centers of hot galaxies (Kormendy & Richstone 1995). Three new BH candidates have been discovered (Ferrarese *et al.* 1996 [NGC 4261]; Kormendy *et al.* 1997 [NGC 4486B]; Bower *et al.* 1997 [NGC 4374]), and the case for 5 more has been strengthened (Harms *et al.* 1994 [M 87], Kormendy *et al.* 1996b [NGC 3115], Kormendy *et al.* 1996c [NGC 4594], Gebhardt *et al.* 1997 [NGC 3377], and van der Marel *et al.* 1997 [M 32]). BHs may play a key role in determining the central structure of galaxies, and no discussion of the central structure expected in HCM models would be complete without examining their influence.

If both BHs and mergers are common among hot galaxies, two galaxies with pre-existing BHs will frequently merge. The BHs will spiral towards the center of the merger remnant, heating and perhaps ejecting the stars. This process may form the observed core in the merger remnant (Begelman *et al.* 1980; Ebisuzaki *et al.* 1991; Makino & Ebisuzaki 1996; Quinlan 1997, Quinlan & Hernquist 1997).

In what follows we assume that every hot galaxy contains a BH with average mass

$$M_{\bullet} = 0.002 M_{gal}, \quad (12)$$

where M_{gal} is the mass of stars in the spheroid. The adopted coefficient 0.002 is a mean of estimates based on the energetics of AGNs and direct mass estimates of local BHs (see Appendix B). The assumption of proportionality in Eq. (12) is motivated by current data on local BHs (Kormendy & Richstone 1995; Kormendy *et al.* 1997), although the measurements show a scatter of at least an order of magnitude.

The evolution of a pair of BHs in a merger remnant was first examined by Begelman *et al.* (1980). A recent comprehensive analysis is provided by Quinlan (1997). The two BHs are carried toward the center of the remnant by the general inward motion of the dense central parts during the merger but will not be exactly at the center at the end of the main merger phase. Subsequent migration of the BHs towards the center occurs on a slower timescale via dynamical friction from the background sea of stars. As the BH orbits decay, they form a bound binary BH whose semi-major axis a continues to shrink through dynamical friction. As the binary becomes more tightly bound, dynamical friction becomes less effective, and the characteristic decay time $|d \log a / dt|^{-1}$ increases. Finally the binary orbit shrinks to the point that gravitational radiation or gas accretion dominates the decay, and rapid coalescence ensues.

Decaying BHs lose most of their energy by heating the surrounding stars. The consequent puffing up of the galaxy was first examined by Ebisuzaki *et al.* (1991). Based on rough analytic arguments and N -body models, they proposed that a merger of two galaxies with BHs would create a low-density core even if none previously existed. They argued that the mass of this core is approximately equal to the sum of the BH masses $M_{\bullet} = m_1 + m_2$. If all galaxies start with the same ratio of BH mass to galaxy mass, this ratio would be unchanged by later merging, and thus the ratios r_b/r_e and M_{\bullet}/M_{gal} would remain constant. This was later seen in hierarchical merging N -body experiments with BHs (Makino & Ebisuzaki 1996) and also agrees approximately with observations (see below).

Quinlan and Hernquist have reexamined the evolution of binary BHs using scattering experiments and N -body models (Quinlan 1997, Quinlan & Hernquist 1997). The following discussion is based on their results, which treat the infall of equal-mass pairs of BHs ranging in individual mass from 0.00125 to $0.04M_{gal}$; the total BH mass $M_{\bullet} = m_1 + m_2$ ranges from 0.0025 to $0.08M_{gal}$. Quinlan has kindly provided details of these models, which allow us to estimate the ratio of BH mass to core mass, a key quantity needed to compare to observations.

The models start with a spherical galaxy whose density profile follows either a Hernquist law,

$$\rho(r) \propto \frac{1}{r(1+r/r_s)^3}, \quad (13)$$

or a modified Hernquist law with steeper slope in the inner parts:

$$\rho(r) \propto \frac{1}{r^{1.5}(1+r/r_s)^{2.5}}. \quad (14)$$

The BHs are started on circular orbits at the half-mass radius r_e of the galaxy. As the BH orbits shrink by dynamical friction, the stellar profiles develop cores. Final break radii r_b were measured (by us) by locating the maximum of the logarithmic curvature of the projected mass surface density, which is equivalent to the definition in the nuker law. We define the indicative core mass as

$$M_{core} \equiv \pi r_b^2 \Sigma(r_b), \quad (15)$$

where $\Sigma(r_b)$ is the projected surface density at r_b . The ratios M_{core}/M_{\bullet} , M_{core}/M_{gal} , and r_b/r_e were tabulated for every model. M_{gal} is the stellar galaxy mass (dark matter is ignored).

The resultant core mass is approximately proportional to the BH mass but depends somewhat on the mean slope of the original mass profile over the region covered by the new core. For M_{\bullet}/M_{gal} near 0.002 (Eq. 12) we find

$$M_{core} = (3.5 - 6.4)M_{\bullet}, \quad (16)$$

which translates to

$$M_{core} = (0.007 - 0.012)M_{gal} \quad (17)$$

if $M_{\bullet}/M_{gal} = 0.002$. The range in parentheses reflects the two models in Eqs. (13) and (14). The scaling relation for break radii analogous to Eq. (17) is found to be

$$r_b = (0.02 - 0.06)r_e. \quad (18)$$

These results imply that the orbital decay of a BH creates an indicative core mass that is 3-6 times the BH mass. This is larger than the core mass $M_{core} \sim M_{\bullet}$ estimated by Ebisuzaki *et al.* (1991), and larger than the ejected mass $M_{ej} \lesssim 2M_{\bullet}$ found by Quinlan & Hernquist. Our explanation is that the ejection of a given mass can create the impression of a more massive core simply due to the precise definition of r_{core} as the point of maximum

logarithmic curvature in the profile — the exact location of r_{core} depends sensitively on how it is defined. The larger indicative core mass in Eq. (16) comes closer to matching the observed indicative core mass for M 87, which is $\sim 10M_{\bullet}$.¹²

The theoretical predictions of Eqs. (17) and (18) are compared to observed core luminosities and break radii in Figs. 9a and 9b. Indicative core luminosity for observed galaxies is defined (analogously to M_{core}) as $L_{core} \equiv \pi r_b^2 I_b$ and is computed from the core parameters in Table 2. The dashed lines are power-law fits to the observed data derived by assuming unit log slope and weighting all points equally. The observed relations are

$$L_{core} = 0.012 L_{gal}, \quad (19)$$

and

$$r_b = 0.03 r_e. \quad (20)$$

The gray areas represent the ranges covered by the theoretical predictions in Eqs. (17) and (18); in plotting Fig. 9a, it is assumed that $M_{core}/M_{gal} = L_{core}/L_{gal}$, which should be true provided $(M/L)_V$ for the stars does not vary strongly between $10''$ and r_e .

Observed core radii are within the range predicted by the models for $M_{\bullet}/M_{gal} = 0.002$, while core luminosities are near the upper boundary of the predicted range. The predicted trends as a function of luminosity are generally matched, although observed core masses may increase as a steeper-than-unity power of total mass (cf. Eq. 8).

The Quinlan-Hernquist models confirm the suggestion (Ebisuzaki *et al.* 1991, Makino & Ebisuzaki 1996) that mergers of galaxies containing massive BHs can generate cores with roughly the size and luminosity indicated by the observations. The presence of BHs in cores also helps to defend cores against accretion: small dense satellites accreted by a primary core galaxy may be disrupted by the BH before they sink to the center.

Despite these encouraging results, models of core formation by massive BHs remain uncertain. In particular, (1) the existing simulations do not yet explore the full range of BH mass ratios and initial conditions appropriate for merging galaxies; and (2) initial BH formation has simply been posited in *ad hoc* fashion in all hot galaxy progenitors (see Haehnelt & Rees 1993).

There are also further problems to be considered:

- (i) Why do core profiles exhibit weak cusps? Perhaps the slow shrinkage of the BH binary naturally forms a cusp, either because the stars are flung into elongated orbits by the binary, or in the same way that cusps are formed when a single central BH grows adiabatically (Peebles 1972; Young 1980; Quinlan, Hernquist & Sigurdsson 1995). However, the N-body models of Quinlan & Hernquist do not show such cusps at present resolution. Alternatively, gas infall into a core previously formed by a BH binary might steepen the profile to create a cusp (Begelman *et al.* 1980; Young 1980). Gas is apparently collecting now at the centers of at least some core galaxies (e.g., M87, Ford *et al.* 1994).

¹² Based on the core parameters of M 87 in Table 2, the fitted nuker-law global M/L_V value for M 87 of 10.2, and $M_{\bullet} = 3 \times 10^9 M_{\odot}$ (Harms *et al.* 1994, as scaled by Kormendy & Richstone 1995).

- (ii) What is the relation of nuclei to BHs? Do they signal BHs, compete with BHs, or possibly feed BHs? The nucleus in NGC 3115 (Kormendy *et al.* 1996b) has a stellar mass of $\sim 3 \times 10^7 M_{\odot}$ crammed into a tiny volume of radius ~ 2 pc around a BH that is 50 times more massive. The stellar density approaches $10^6 M_{\odot} \text{pc}^{-3}$, and typical orbital velocities exceed 1000 km s^{-1} . It is a puzzle how stars could have formed in such an environment, where gas clouds are likely to be colliding at high velocities while bathed by intense radiation from the BH. Perhaps the nucleus and BH formed in different progenitors that later merged.
- (iii) Our discussion so far has stressed correlations of core and global properties. In fact there are outliers such as Fornax A, which has a very small core for its luminosity (Fig. 4a). Fornax A is peculiar and is probably still in the throes of a major merger (Schweizer 1980). Perhaps the inner regions have not yet settled down to their final state, giving us a clue to the time scales involved in core scouring; or gas (as signaled by the copious dust) may be (re)forming a stellar cusp, although there is no sign of young stars in the color map (Shaya *et al.* 1996).
- (iv) BHs appear to be associated with the hot component of spiral galaxies; late-type spirals such as M33 have little or no central BH (Kormendy & McClure 1993). When two late-type galaxies merge, they are believed to form an elliptical, but this will not have the central BH that is required for core formation in subsequent hierarchical merging.
- (v) Most important, if cores are formed by merging binary BHs, why do power-law galaxies at intermediate magnitudes ($-20.5 > M_V > -22$) not have cores with size as given by Eq. (18)? BHs appear to be just as common in power-law galaxies (Kormendy & Richstone 1995). Perhaps power laws can be regenerated by star formation from fresh gas supplied by the latest merger. However, to avoid being ejected by the BH binary, the new stars must form *after* the BH binary shrinks, which poses a timing problem if BHs sink to the center more slowly than gas.

9. SUMMARY AND CONCLUSIONS

We have assembled inner surface-brightness profiles for 61 dynamically hot galaxies available in the HST archive as of June 1993. Fits of the nuker law (Eq. 2) to deconvolved profiles are used to compute values of break radius r_b and break surface brightness I_b . These are supplemented with ground-based data from the literature on rotation, isophote shape, and velocity dispersion. These data are used to produce updated versions of the central parameter diagrams for hot galaxies.

The inner surface-brightness profiles of hot galaxies can be divided into two types as discussed in Paper I. *Core* galaxies have a sharp knee or bend in the profile, akin to the analytic cores of King models or the isothermal sphere but with a shallow cusp at small radii. *Power-law* galaxies have profiles that are steep and rather featureless in log-log coordinates with no detectable core at $0''.1$ resolution.

Cores appear only in galaxies brighter than $M_V = -20.5$ (Fig. 4a); core size and luminosity are roughly proportional to galaxy size and luminosity (Eqs. 18 and 19). Power-law galaxies are fainter than $M_V = -22$. In the overlap region from $M_V = -20.5$ to -22 , the two types coexist and profile morphologies vary widely — upper limits to core size in some power-law galaxies are at least 100 times smaller than the core sizes of other galaxies at the same luminosity.

The scatter in central properties in the overlap region correlates with global structure: core galaxies tend to be boxy and rotate slowly, while power-law galaxies are disk-like and rotate rapidly. Preliminary evidence suggests a further correlation with environment in that core galaxies tend to be found in dense groups and clusters while bright power laws are preferentially found in the field.

Cores populate a fundamental plane (FP) that is analogous to and roughly parallel to the global FP for elliptical galaxies. The scatter about this plane (in $\log r_b$) is 0.12 dex, about 30% larger than the analogous scatter about the global FP. Some of this extra scatter may come from massive BHs, which may inflate central velocity dispersions in some galaxies.

A set of self-consistent scaling relations for core galaxies is presented that expresses core size, density, and other quantities as a function of L_V (Eqs. 3–10). These scaling laws are projections of the FP. A major conclusion is that small hot galaxies are much denser than large ones, by a factor of up to 1000 at a radius of 10 pc.

The last part of the paper attempts to relate the central parameter relations of hot galaxies to the process of galaxy formation and evolution. We suggest that the presence of dense power-law centers, disk-like isophotes, and rapid rotation in low-luminosity galaxies all point to their formation via *dissipative, gas-rich mergers*. The analogous arguments about core galaxies are less clear: the boxy isophote shape and slow rotation of these luminous objects suggest formation by *dissipationless* mergers, but cores may be difficult to form and maintain in such events. For example, core galaxies seem at present to be accreting small dense satellites in sufficient numbers to fill in their low-density cores, at least if the satellites survive their orbital decay to the center, an issue that is still in dispute.

We explore an alternative model for core formation based on merging BHs. The model assumes that BH binaries are formed in galaxy mergers; the binary orbit decays by dynamical friction, ejecting stars from the center of the merger remnant, enlarging any previous core, and scouring out a new one where none existed. Simulations of this process by Quinlan & Hernquist (1997) yield a reasonable match to the radii and masses of observed cores if every hot galaxy contains a central BH of average mass $M_\bullet = 0.002 M_{gal}$. This value for M_\bullet is consistent with BH mass estimates in AGNs and local BHs (see Appendix B). Whether or not BHs are the dominant agent in creating cores, their role in shaping the central structure of hot galaxies is likely to be significant if they are as common and as massive as recent estimates suggest.

The main goal of this paper is to explore systematic trends in the central structure of hot galaxies and the possible relations between their present central structure and their formation history. By strengthening the link between the central structures of hot galaxies and their global properties such as luminosity, shape, and rotation, *HST* has helped to open an important new window on galaxy formation.

We would especially like to thank Martin Weinberg and Gerry Quinlan for informative discussions on satellite capture and survival and for providing pre-publication accounts of their calculations. John Tonry provided distance estimates to many galaxies in advance of publication, for which we are very grateful. The referee made several very helpful suggestions. During the last five years, our team has been hosted by Prof. James Westphal of Caltech, the Institute for Astronomy at the University of Hawaii, the Observatories of the Carnegie Institution of Washington, the Institute for Theoretical Physics at UCSB, the National Optical Astronomy Observatories, the Aspen Center for Physics, and the Fields Institute for Research in Mathematical Sciences at the University of Toronto. We thank them for their gracious hospitality. Our collaboration was supported by *HST* data analysis funds through GO grants GO-2600.01.87A and GO-06099.01-94A, by NASA grant NAS-5-1661 to the WFPC1 IDT, and by grants from NSERC.

APPENDIX A: THE NATURE OF POWER LAWS AND THE FREQUENCY OF INNER DISKS IN POWER-LAW GALAXIES

Jaffe *et al.* (1994) and Ferrarese *et al.* (1994), like us, divide hot galaxies into two types based on inner surface-brightness profile. Those called by us *cores* with a strong break and low central surface brightness they term Type I, and those called by us *power-laws* with no break and high central surface they call Type II. There is no discrepancy between us as to division into classes based on profile shape.

Jaffe *et al.* go on to identify core galaxies in a general way with slowly rotating boxy galaxies, and power-law galaxies with rotating disk galaxies. This distinction resembles ours but differs in important details. For example, Jaffe *et al.* envision that the centers of hot galaxies either have or do not have small *inner disks*. Such disks *seen edge-on* are what create the high surface brightness power-law profiles of Type II galaxies. These inner disks are furthermore associated with the global, outer disks of rotating disk galaxies. It is the frequent association between inner disks and outer disks that creates the link between power-law profiles and disk rotating galaxies in their picture.

Jaffe *et al.* believe that the high surface brightness profiles of power-law galaxies are produced *only* when an inner disk is seen edge-on. Specifically they state: “Most of the characteristics. . .that discriminate Type I from Type II are explained by disk components seen at high inclination angles. For example, the higher central surface brightness in Type II systems is caused by the nuclear disk seen close to edge-on. . .If one of these [disky] galaxies [i.e., a Type II] were viewed face on, it would appear much more like a Type I galaxy.” Thus, their view is that observed profile type is due to a combination of intrinsic properties plus viewing aspect. All power-laws have inner disks – they are the disks that happen to be seen edge-on. Core-type profiles on the other hand are a mixture; many are intrinsic cores that lack inner disks, while some fraction are disks seen face-on that are masquerading as cores.

This interpretation of cores versus power laws differs importantly from our own. Our view is that the difference between core and power-law profiles is intrinsic to the *hot* stellar component and has no direct connection with a disk, whether seen edge-on or face-on. Power laws remain power laws at any viewing angle, as do cores. Paper I presented initial arguments against the edge-on disk explanation for power laws. We have since undertaken a more comprehensive comparison with power-law galaxies in the present data set. Briefly, we find that the small sample of Virgo galaxies analyzed by Jaffe *et al.* was abnormally dominated by late-type edge-on S0 galaxies. Nearly every power-law galaxy they detected was such an object. A high frequency of edge-on *inner* disks in such a sample is therefore understandable. Our sample is larger and contains many power-law ellipticals that are not flattened and show no sign of either an inner or an outer disk. This and other evidence to be described leads us to conclude that power-laws are independent of inner disks and are thus a feature of the hot stellar component alone.

We carefully examined deconvolved V-band images of all 61 galaxies in the present sample. Thirteen of the 14 Jaffe *et al.* galaxies were available in the archive, and we looked at all of them. Seven of these were admitted into our sample (they are included in Table 1). The remaining six galaxies were rejected for the following reasons: (1) too much

dust to derive a reliable surface-brightness profile or class the object as a core or power law (NGC 4261, NGC 4342, NGC 4374, NGC 4476); (2) a potential double nucleus and unclassifiable profile (NGC 4473); (3) no clear spheroidal component (NGC 4550); and (4) interfering spiral arms (NGC 4476). Compared to our sample, the Jaffe *et al.* power-law galaxies are much later in type, diskier, more edge-on, and more subject to dust and other peculiarities that potentially interfere with reliable measurement of the spheroid profile.

If the edge-on disk interpretation were correct, then all or most power-law galaxies in our sample should show evidence of disks. To test this, we inspected each image within a $10''$ radius for an inner disk comprised of either stars or dust. We also looked for spiral arms, which we took as another indicator of a disk. We visually assessed isophote shape as a function of radius, checking for changes and comparing to measured values of a_4 . We tried to correlate changes in ellipticity and shape with kinks or “ledges” in the brightness profile — such correlations might signify the edge of a disk. We also subtracted the profile fits given in Paper I and looked for signs of a residual disk. Table 4 summarizes the results of this visual inspection. On the basis of this evidence, we assigned a final score to each galaxy indicating the likelihood of an *inner* disk. The values are 0 (no sign of a disk), 1 (possible disk), 2 (probable disk), and 3 (disk plainly visible). These scores are given in the table, along with comments.

The results of these efforts are summarized in Fig. 10, which plots inner disk score versus ellipticity for power-law galaxies. The hypothesis that *all* power-law objects have edge-on inner disks seems unlikely because: (1) Half the sample shows little or no evidence of any inner disk, including several highly flattened objects. (2) Power-law galaxies are not concentrated at high ellipticities, in contrast to the sample of Jaffe *et al.* (3) Most objects with inner disks are bulges that also have outer disks (types S0, Sa, or Sb), a point also made by Jaffe *et al.* However, this weakens the case for ubiquitous inner disks in power-law *ellipticals* because they lack such outer disks. (4) One power-law galaxy, NGC 3599, shows face-on spiral structure, showing conclusively that it cannot be edge-on. (5) If known bulges are excluded, the ellipticity distribution of the remaining power-law ellipticals is nearly the same as that of core ellipticals (which lie within the rectangle in Fig. 10 but are not plotted individually), and neither type shows much evidence for inner disks. Thus the evidence for inner disks is weak in both power-law and core ellipticals.

A less restrictive hypothesis, not put forward by Jaffe *et al.*, is that power laws are associated with a high surface-brightness inner disk, period, whether seen *either* edge-on or face-on. This also seems unlikely because there are several flattened power-law ellipticals that must be close to edge-on yet show no sign of a disk (point 1 above). The kinematic properties of M 31 and M 32 are also relevant here. Both of these would be typical power laws if seen at a distance, yet both are hot and slowly rotating at radii of a few arcsec, the claimed size of inner disks in other power-law galaxies. In neither galaxy is there any hint from kinematics that the high central surface brightness is associated with a disk.

To summarize, present evidence does not favor the ubiquitous presence of high surface-brightness *inner* disks in power-law galaxies, whether edge-on or not, though such disks are certainly present in some cases. Rather we believe that the difference between core and power-law profiles more probably reflects an intrinsic difference in the *spheroidal* light

distribution between the two types. Finally we note cautiously that one of our low-disk-score galaxies, NGC 3377 (disk score = 1), has since revealed a dust disk in recent WFPC2 images. Final conclusions about the frequency of inner disks in ellipticals and bulges should therefore await a new body of high-quality WFPC2 images.

APPENDIX B: THE MEAN BH MASS PER HOT GALAXY

The following argument adapted from Tremaine (1997) summarizes the evidence for the frequency and masses of BHs in the centers of hot galaxies.

The integrated comoving energy density in quasar light (as emitted) is (Chokshi & Turner 1992)

$$u = 1.3 \times 10^{-15} \text{ erg cm}^{-3}, \quad (21)$$

independent of H_0 and Ω . If this energy is produced by burning fuel with an assumed efficiency $\epsilon \equiv \Delta E / (\Delta M c^2)$, then the mean mass density of dead quasars must be at least (Soltan 1982, Chokshi & Turner 1992)

$$\rho_{\bullet} = \frac{u}{\epsilon c^2} = 2.2 \times 10^5 \left(\frac{0.1}{\epsilon} \right) M_{\odot} \text{ Mpc}^{-3}, \quad (22)$$

assuming that the Universe is homogeneous and transparent.

The mass of a dead quasar may be written

$$M_{\bullet} = \frac{L_Q \tau}{\epsilon c^2} = 7 \times 10^8 M_{\odot} \left(\frac{L_Q}{10^{12} L_{\odot}} \right) \left(\frac{\tau}{10^9 \text{ y}} \right) \left(\frac{0.1}{\epsilon} \right), \quad (23)$$

where L_Q is the quasar luminosity and τ is its lifetime. An upper limit to the lifetime is the evolution timescale for the quasar population as a whole, $\sim 10^9$ y; however, upper limits to BH masses in nearby galaxies and direct estimates of the BH masses in AGNs both suggest that the actual masses and lifetimes are smaller by a factor 10-100 (Haehnelt & Rees 1993), which implies $M_{\bullet} = 10^7$ – $10^8 M_{\odot}$.

To focus discussion, we adopt a strawman model in which a fraction f of all galaxies contains a central BH, and BH mass is proportional to galaxy luminosity. Thus $M_{\bullet} = \Upsilon L$, where Υ is the (black hole) to (galaxy) mass-to-light ratio. The luminosity density of galaxies is $j = 1.5 \times 10^8 L_{\odot} \text{ Mpc}^{-3}$ in the blue band (Efstathiou *et al.* 1988, adjusted to our Hubble constant of $H_0 = 80 \text{ km s}^{-1} \text{ Mpc}^{-1}$). Thus

$$\Upsilon = \frac{\rho_{\bullet}}{f j} = \frac{0.0015}{f} \left(\frac{0.1}{\epsilon} \right) \frac{M_{\odot}}{L_{\odot}}. \quad (24)$$

This value is an average over the light of all local galaxies. However, if we assume that massive BHs are found chiefly in the centers of hot galaxies (Kormendy & Richstone 1995), the above number can be converted to the BH mass-to-light ratio *per hot component* by

noting that approximately 30% of the local B-band light is emitted by such components (Schechter & Dressler 1987). Correcting for this and converting to the V band yields

$$\Upsilon_V^h = \frac{0.004}{f_h} \left(\frac{0.1}{\epsilon} \right) \frac{M_\odot}{L_\odot}, \quad (25)$$

where Υ_V^h is now the estimated ratio M_\bullet/L_V per hot component and f_h is the fraction of *hot galaxies* with BHs.

A second estimate of Υ_V^h from quasars comes from dividing the typical dead quasar mass derived above, $M_\bullet \approx 10^{7.5} M_\odot$, by the typical luminosity of a bright hot component, $8.5 \times 10^9 L_\odot$ (Binggeli, Sandage & Tammann 1988, adjusted to $H_0 = 80 \text{ km s}^{-1} \text{Mpc}^{-1}$). The result is $\Upsilon_V^h \approx 0.004$. Consistency with Eq. (25) then requires $f_h \approx 1$ if $\epsilon \approx 0.1$, or that most or all hot galaxies contain a BH.

A final method for estimating Υ_V^h uses individual BH masses for 6 moderately well established BHs in nearby hot galaxies¹³ (Kormendy & Richstone 1995, Table 1). Using an estimate of global stellar M/L_V based on nuker-law fits as described in Table 3¹⁴ yields the logarithmic mean value $\Upsilon_V^h = 0.016$. This is in reasonable agreement with $\Upsilon_V^h = 0.004$ from quasars in view of the likelihood that these best BH candidates are more massive than average.

For further discussion, we assume that every hot galaxy contains a BH and adopt for Υ_V^h the logarithmic mean of the quasar and BH values:

$$\Upsilon_V^h = 0.008. \quad (26)$$

The corresponding value of M_\bullet/M_{gal} is then

$$M_\bullet/M_{gal} = 0.002, \quad (27)$$

where M_{gal} comes from $L_V(M/L)_V$ and $(M/L)_V$ is the above-mentioned mean global mass-to-light ratio for the 6 candidate BH galaxies. This is the value of M_\bullet/M_{gal} per hot component adopted in Section 8.

¹³ The Galaxy and NGC 4258 are omitted for lack of accurate luminosities of their hot components, and NGC 3115 uses the new value of $M_\bullet = 2 \times 10^9 M_\odot$ from Kormendy *et al.* (1996b).

¹⁴ For the present purpose, the mass fits were renormalized to fit σ at $10''$ using the ratio $R_\sigma = \sigma(10'')/\sigma_0$ from Table 2. This was done to avoid possible contamination of σ_0 by a BH. The logarithmically averaged (M/L_V) for the 6 galaxies is 4.0 in solar units ($H_0 = 80 \text{ km s}^{-1} \text{Mpc}^{-1}$).

REFERENCES

- Balcells, M., & Quinn, P. J. 1990, *ApJ*, 361, 381
- Bardeen, J. M., Bond, J. R., Kaiser, N., & Szalay, A. S. 1986, *ApJ*, 304, 15
- Barnes, J. E. 1988, *ApJ*, 331, 699
- Barnes, J. E. 1992, *ApJ*, 393, 484
- Barnes, J. E. 1996, in *New Light on Galaxy Evolution*, IAU Symposium No. 171, eds. R. Bender & R. L. Davies (Kluwer, Dordrecht), 191
- Barnes, J. E., & Hernquist, L. 1991, *ApJ*, 370, L65
- Barnes, J. E., & Hernquist, L. 1992, *ARA&A*, 30, 705
- Barnes, J. E., & Hernquist, L. 1996, *ApJ*, 471, 115
- Begelman, M. C., Blandford, R. D., & Rees, M. J. 1980, *Nature*, 287, 307
- Bender, R. 1988, *A&A*, 193, L7
- Bender, R., Burstein, D., & Faber, S.M. 1992, *ApJ*, 399, 462
- Bender, R., & Möllenhoff, C. 1987, *A&A*, 177, 71
- Bender, R., & Nieto, J.-L. 1990, *A&A*, 239, 97
- Bender, R., Saglia, R. P., & Gerhard, O. E. 1994, *MNRAS*, 269, 785
- Bender, R., & Surma, P. 1988, *A&A*, 258, 250
- Bender, R., & Surma, P. 1995, *A&A*, 298, 405
- Bender, R., Surma, P., Döbereiner, S., Möllenhoff, C., & Madejsky, R. 1989, *A&A*, 217, 35
- Bertola, F., Capaccioli, M., Galletta, G., & Rampazzo, R. 1988, *A&A*, 192, 24
- Binggeli, B., & Cameron, L. M. 1993, *A&AS*, 98, 297
- Binggeli, B., Sandage, A. R., & Tammann, G. A. 1985, *AJ*, 90, 168
- Binggeli, B., Sandage, A. R., & Tammann, G. A. 1988, *ARA&A*, 26, 509
- Binney, J., Davies, R. L., & Illingworth, G. D. 1990, *ApJ*, 361, 78
- Binney, J., & Petrou, M. 1985, *MNRAS*, 214, 449

- Binney, J. & Tremaine, S. 1987, *Galactic Dynamics* (Princeton University Press, Princeton), 514
- Blumenthal, G., Faber, S. M., Primack, J., & Rees, M. J. 1984, *Nature*, 311, 517
- Boroson, T. 1981, *ApJS*, 46, 177
- Bosma, A. Smith, R. M., & Wellington, K. J. 1985, *MNRAS*, 212, 301
- Bower, G., *et al.* 1997, in preparation
- Burkhead, M. 1986, *AJ*, 128, 465
- Burstein, D. 1979, *ApJ*, 234, 435
- Bushouse, H. A. 1987, *ApJ*, 320, 49
- Byun, Y.-I., *et al.* 1996, *AJ*, 111, 1889 (Paper II)
- Capaccioli, M., Held, E. V., & Nieto, J.-L. 1987, *AJ*, 94, 1519
- Carlberg, R. 1986, *ApJ*, 310, 593
- Chokshi, A., & Turner, E. L. 1992, *MNRAS*, 259, 421
- Condon, J. J., Huang, Z.-P., Yin, Q. F., & Thuan, T. X. 1991, *ApJ*, 378, 65
- Crane, P. *et al.* 1993, *AJ*, 106, 1371
- Davies, R. L., & Birkinshaw, M. 1988, *ApJS*, 68, 409
- Davies, R. L., Efstathiou, G., Fall, S. M, Illingworth, G. D., & Schechter, P. L. 1983, *ApJ*, 266, 41
- Davies, R. L., & Illingworth, G. D. 1983, *ApJ*, 266, 516
- de Vaucouleurs, G. 1958, *ApJ*, 128, 465
- de Vaucouleurs, G., de Vaucouleurs, A., Corwin, H. G., Buta, R. J., Paturel, G., & Fouqué, P. 1991, *Third Reference Catalogue of Bright Galaxies* (Springer, New York) (RC3)
- de Vaucouleurs, G., de Vaucouleurs, A., & Corwin, H. G., 1976, *Second Reference Catalogue of Bright Galaxies* (Univ. of Texas Press, Austin) (RC2)
- de Zeeuw, T. & Franx, M. 1991, *ARA&A*, 29, 239
- Djorgovski, S., & Davis, M. 1987, *ApJ*, 313, 59

- Dressler, A., Lynden-Bell, D., Burstein, D., Davies, R. L., Faber, S. M., Terlevich, R., & Wegner, G. 1987, ApJ, 313, 42
- Dressler, A. & Richstone, D. O. 1988, ApJ, 324, 701
- Dressler, A. & Richstone, D. O. 1990, ApJ, 348, 120
- Dubinski, J. 1997, in preparation
- Ebisuzaki, T., Makino, J., & Okumura, S. K. 1991, Nature, 354, 212
- Efstathiou, G., Ellis, R. S., & Carter, D. 1980, MNRAS, 193, 931
- Efstathiou, G., Ellis, R. S., & Carter, D. 1982, MNRAS, 201, 975
- Efstathiou, G., Ellis, R. S., & Peterson, B. A. 1988, MNRAS, 232, 431
- Faber, S. M. 1973, ApJ, 179, 423
- Faber, S. M., Dressler, A., Davies, R. L., Burstein, D., Lynden-Bell, D., Terlevich, R., & Wegner, G. 1987, in *Nearly Normal Galaxies: From the Planck Time to the Present*, ed. S. M. Faber (Springer, New York), 175
- Faber, S. M., Wegner, G., Burstein, D., Davies, R. L., Dressler, A., Lynden-Bell, D., & Terlevich, R. J. 1989, ApJS, 69, 763
- Farouki, R. T., Shapiro, S. L., & Duncan, M. J. 1983, ApJ, 265, 597
- Ferrarese, L., van den Bosch, F. C., Ford, H. C., Jaffe, W., & O'Connell, R. W. 1994, AJ, 108, 1598
- Ferrarese, L., Ford, H. C., Jaffe, W., 1996, ApJ, 470, 444
- Fisher, D., Illingworth, G. D., & Franx, M. 1995, ApJ, 438, 539
- Forbes, D. A., Franx, M., & Illingworth, G. D. 1994, ApJ, 428, L49
- Forbes, D. A., Franx, M., & Illingworth, G. D. 1995, AJ, 109, 1988
- Ford, H. C., *et al.* 1994, ApJ, 435, L27
- Franx, M., & Illingworth, G. D. 1988, ApJ, 327, L55
- Franx, M., Illingworth, G. D., & Heckman, T. 1989a, ApJ, 344, 613
- Franx, M., Illingworth, G. D., & Heckman, T. 1989b, AJ, 98, 538
- Fried, J. W., & Illingworth, G. D. 1994, AJ, 107, 992

- Gebhardt, K. *et al.* 1996, AJ, 112, 105 (Paper III)
- Gebhardt, K. *et al.* 1997, in preparation
- Gonzalez, J. J. 1993, Ph.D. thesis, University of California, Santa Cruz
- Goudfrooij, P., Hansen, L., Jørgensen, H. E., Nørgaard-Nielsen, H. U., de Jong, T., & van den Hoek, L. B. 1994, A&AS, 104, 179
- Grillmair, C. J., *et al.* 1994, AJ, 108, 102
- Haehnelt, M. G., & Rees, M. J. 1993, MNRAS, 263, 168
- Harms, R. J., *et al.* 1994, ApJ, 435, L35
- Hernquist, L. 1993, ApJ, 409, 548
- Hernquist, L., & Barnes, J. E. 1991, Nature, 354, 210
- Hoessel, J. G., Gunn, J. E., & Thuan, T. X. 1980, ApJ, 241, 486
- Jaffe, W., Ford, H. C., O'Connell, R. W., van den Bosch, F. C., & Ferrarese, L. 1994, AJ, 108, 1567
- Jaffe, W., Ford, H. C., Ferrarese, L., van den Bosch, F. C., & O'Connell, R. W. 1996, ApJ, 460, 214
- Jarvis, B. J., & Freeman, K. C. 1985, ApJ, 295, 324
- Jedrzejewski, R. I., & Schechter, P. L. 1988, ApJ, 330, L87
- Jedrzejewski & Schechter, P. L. 1989, AJ, 98, 147
- Kauffmann, G. 1996, MNRAS, 281, 487
- Kennicutt, R. C., Keel, W. C., van der Hulst, J. M., Hummel, E., & Roettiger, K. A. 1987, AJ, 93, 1011
- Kent, S. M., 1983, ApJ, 266, 562
- Kormendy, J. 1977, ApJ, 217, 406
- Kormendy, J. 1982a, in Morphology and Dynamics of Galaxies, eds. L. Martinet & M. Mayor (Sauverny: Geneva Observatory), 113
- Kormendy, J. 1982b, ApJ, 257, 75
- Kormendy, J. 1984, ApJ, 287, 577

- Kormendy, J. 1985, ApJ, 295, 73
- Kormendy, J. 1987a, in IAU Symposium 127, Structure and Dynamics of Elliptical Galaxies, ed. T. de Zeeuw (Reidel, Dordrecht), 17
- Kormendy, J. 1987b, in Nearly Normal Galaxies: From the Planck Time to the Present, ed. S. M. Faber (Springer, New York), 163
- Kormendy, J. 1988, ApJ, 325, 128
- Kormendy, J. 1989, ApJ, 342, L63
- Kormendy, J., & Bender, R. 1996, ApJ, 464, L119
- Kormendy, J., & Djorgovski, S. 1989, ARA&A, 27, 235
- Kormendy, J., Dressler, A., Byun, Y.-I., Faber, S. M., Grillmair, C., Lauer, T. R., Richstone, D. O., & Tremaine, S. 1994, in ESO/OHP Workshop on Dwarf Galaxies, eds. G. Meylan & P. Prugniel (Garching: ESO), 147
- Kormendy, J., & Illingworth, G. 1983, ApJ, 265, 632
- Kormendy, J., & McClure, R. D. 1993, AJ, 105, 1793
- Kormendy, J., & Richstone, D. O. 1992, ApJ, 393, 559
- Kormendy, J., & Richstone, D. 1995, ARA&A, 33, 581
- Kormendy, J., & Sanders, D. B. 1992, ApJ, 390, L53
- Kormendy, J., & Westpfahl, D. J. 1989, ApJ, 338, 752
- Kormendy, J., *et al.* 1996a, in New Light on Galaxy Evolution, IAU Symposium No. 171, eds. R. Bender & R. L. Davies (Kluwer, Dordrecht), 105
- Kormendy, J., *et al.* 1996b, ApJ, 459, L57
- Kormendy, J., *et al.* 1996c, ApJ, 473, L91
- Kormendy, J., *et al.* 1997, ApJ, 482, L139
- Larson, R. B. 1974a, MNRAS, 166, 585
- Larson, R. B. 1974b, MNRAS, 169, 229
- Lauer, T. R. 1983, Ph.D. Thesis, University of California, Santa Cruz
- Lauer, T. R. 1985a, ApJ, 292, 104

Lauer, T. R. 1985b, MNRAS, 216, 429

Lauer, T. R. 1988, ApJ, 325, 49

Lauer, T. R., *et al.* 1991, ApJ, 369, L41

Lauer, T. R., *et al.* 1992a, AJ, 104, 552

Lauer, T. R., *et al.* 1992b, AJ, 103, 703

Lauer, T. R., *et al.* 1993, AJ, 106, 1436

Lauer, T. R., *et al.* 1995, AJ, 110, 2622 (Paper I)

Lauer, T. R., *et al.* 1996, ApJ, 471, L79

Lauer, T. R., *et al.* 1997, in preparation

Leech, K. J., Penston, M. V., Terlevich, R., Lawrence, A., Rowan-Robinson, M., & Crawford, J. 1989, MNRAS, 240, 349

Lugger, P. M., Cohn, H., Cederbloom, S. E., Lauer, T. R., *et al.* 1992, AJ, 104, 83

Lynden-Bell, D., Faber, S. M., Burstein, D., Davies, R. L., Dressler, A., Terlevich, R. J., & Wegner, G. 1988, ApJ, 326, 19

Makino, J., & Ebisuzaki, T. 1996, ApJ, 465, 527

Merritt, D. 1985, ApJ, 289, 18

Mihos, J. C., & Hernquist, L. 1994, ApJ, 437, L47

Negroponte, J., & White, S. D. M. 1983, MNRAS, 205, 1009

Nieto, J.-L. 1988, Bol. Acad. Nac. Cine. Cordoba, 58, 239

Nieto, J.-L., & Bender, R. 1989, A&A, 215, 266

Nieto, J.-L., Bender, R., & Surma, P. 1991a, A&A, 244, L37

Nieto, J.-L., Bender, R., Arnaud, J., & Surma, P. 1991b, A&A, 244, L25

Nieto, J.-L., Poulain, P., Davoust, E., Rosenblatt, P. 1991c, A&AS, 88, 559

Ostriker, J. P. 1980, Comm. Astrophys., 8, 177

Peebles, P. J. E. 1972, Gen. Rel. Grav. 3, 63

- Peletier, R. F. Davies, R. L. Illingworth, G. D., Davis, L. E. 1990, AJ, 100, 1091
- Quinlan, G. D. 1997, New Astron. 1, 35
- Quinlan, G. D., & Hernquist, L. 1997, submitted to New Astronomy
- Quinlan, G. D., Hernquist, L., & Sigurdsson, S. 1995, ApJ, 440, 554
- Minske, K., & Richstone, D. O. 1997, in preparation
- Sanders, D. B., Soifer, B. T., Elias, J. H., Madore, B. F., Mathews, K., Neugebauer, G., & Scoville, N. Z. 1988, ApJ, 325, 74
- Schechter, P. L., & Dressler, A. 1987, AJ 94, 563
- Schweizer, F. 1980, ApJ, 237, 303
- Schweizer, F. 1986, Science, 231, 227
- Schweizer, F., Seitzer, P., Faber, S. M., Burstein, D., Dalle Ore, C. M., & Gonzalez, J. J. 1990, ApJ, 364, L33
- Scorza, C., & Bender, R. 1995, A&A, 293, 20
- Scoville, N. Z., Sargent, A. I., Sanders, D. B., & Soifer, B. T. 1991, ApJ, 366, L5
- Shaya, E. J., *et al.* 1996, AJ, 111, 2212
- Simien, F., & de Vaucouleurs, G. 1986, ApJ, 302, 564
- Solomon, P. M., Downes, D., & Radford, S. J. E. 1992, ApJ, 387, L55
- Sołtan, A. 1982, MNRAS, 200, 115
- Tonry, J. 1984, ApJ, 283, L27
- Toomre, A. 1977, in *The Evolution of Galaxies & Stellar Populations*, eds. B. M. Tinsley & R. B. Larson (Yale, New Haven), 401
- Tremaine, S. 1976, ApJ, 203, 345
- Tremaine, S. 1997, in *Unsolved Problems in Astrophysics*, eds. J. N. Bahcall and J. Ostriker (Princeton University Press, Princeton), p. 137
- van den Bosch, F. C., Ferrarese, L., Jaffe, W., Ford, H. C., & O'Connell, R. W. 1994, AJ, 108, 1579

- van der Marel, R. P. 1991, MNRAS, 253, 710
- van der Marel, R. P., Rix, H.-W., Carter, D., Franx, M., White, S. D. M., de Zeeuw, T. 1994, MNRAS, 268, 521
- van der Marel, R. P., de Zeeuw, T., Rix, H.-W., & Quinlan, G. D. 1997, Nature, 385, 610 *et al.* 1996,
- Weil, M. & Hernquist. L. 1996, ApJ, 460, 101
- Weinberg, M. D. 1994, AJ, 108, 1398
- Weinberg, M. D. 1997, ApJ, 478, 435
- White, S. D. M., & Rees, M. J. 1978, MNRAS, 183, 341
- Whitmore, B., McElroy, D. B., & Tonry, J. L. 1985, ApJS, 59, 1
- Young, P. J. 1980, ApJ, 242, 1232
- Young, P. J., Westphal, L. A., Kristian, J., Wilson, C. P., & Landauer, F. P. 1978, ApJ, 221, 721

FIGURES

Figure 1: V-band surface-brightness profiles of 55 ellipticals and bulges from *HST*. All were observed in the WFPC1 Planetary Camera through filter F555W and were deconvolved using the Lucy-Richardson algorithm as described in Paper I. Core galaxies (see Section 2) are plotted as solid lines, and power-law galaxies are plotted as dashed lines. “Mean radius” is the geometric mean of the semi-major and semi-minor axes of the isophotal ellipse.

Figure 2: *HST* surface-brightness profiles of M 31 and M 32, as seen locally and near Virgo (24 times farther). To simulate Virgo, the nearby profile was binned by a factor of 24, convolved with the WFPC1 point-spread function, and deconvolved with 80 iterations of the Lucy-Richardson algorithm.

Figure 3: Division of the sample into cores and power laws. The figure plots logarithmic inner slope of the surface-brightness profile, γ , versus angular break radius, θ_b , from fits to the nuker law (Eq. 2). Galaxies with $\log \theta_b > -0.8$ are well resolved and divide into two groups with high and low γ . Dashed lines connecting the near and far versions of M 31 and M 32 indicate potential resolution effects on other power-law galaxies. A galaxy must have $\gamma < 0.3$ and a well-resolved break radius to be classed as a core. Galaxies within the box comprise the “Core” sample.

Figure 4: *HST* measurements of central parameters of hot galaxies, as a function of absolute V magnitude. Hubble type and nucleus types are taken from Table 1; “bulges” are S0–Sb galaxies. r_b and μ_b for power laws are limits r_b^{lim} and μ_b^{lim} from Table 2. M 31 and M 32 are plotted twice: asterisks show data as observed, and tails indicate their positions as they would appear 24 times farther away near Virgo. The small black square is the S0 galaxy NGC 524, which is the only core within a bulge. The apparent turndown in surface brightness at faint magnitudes in panel (c) is probably a resolution effect (cf. M 32). Effective radii are plotted in panel (d), to be compared with break radii in panel (a): the strong impressions of scatter at intermediate magnitudes ($-22 < M_V < -20.5$) and of two types of galaxies in panel (a) are absent in panel (d).

Figure 5: Break radius r_b versus distance. The dashed line is the adopted dividing line for cores in Fig. 3 ($\log \theta_b = -0.8$). Above this line, a core-type profile will be seen as a resolved core, below it will be classed as a power-law. The trend versus distance is opposite to what one would have expected if cores and power-laws were merely an artifact of angular resolution — core galaxies are on average *more* distant than power-laws. Moreover, most of the sample is close to Virgo in distance ($\log D \sim 3.2$), yet contains both cores and power laws, confirming that the two types are intrinsically different.

Figure 6: Various densities at radius $0''.1$ plotted against absolute magnitude. Mass densities are derived by normalizing nuker-law surface-brightness fits to central σ_0 . The symbols are the same as in Fig. 4. Model details are given in the text and notes to Table

3. Panel (a) luminosity density; panel (b) mass density; panel (c) peak Maxwellian phase-space density. Note the range of almost 10^6 in density in all three panels. Turndowns for small galaxies are probably an artifact of resolution (cf. M 32).

Figure 7a: Replot of Fig. 4a with symbols indicating rotation speed $(v/\sigma)_*$. Slow rotators (filled symbols) have $(v/\sigma)_* < 0.51$; fast rotators (open circles) have $(v/\sigma)_* \geq 0.51$. Bulges lacking data are classed as fast rotators. Galaxies with core profiles are indicated by the enclosing squares; all others are power laws. The data indicate a tendency for fast rotators to have power-law profiles.

Figure 7b: Same as Fig. 7a but with symbols indicating isophotal shape a_4/a . Galaxies are classed as disk if $a_4/a \geq 0.4$, otherwise as boxy/neutral. Irregular profiles with variable a_4/a are also classed as boxy/neutral. Bulges (Hubble types S0–Sb) are classed as disk. The data indicate a tendency for disk galaxies to have power-law profiles.

Figure 8: *HST* measurements of central parameters of hot galaxies in fundamental-plane space. Symbols are the same as in Fig. 4. Tails on M 31 and M 32 (asterisks) show the effect of moving these galaxies 24 times further away to the vicinity of Virgo. Resolution effects on other power-law galaxies may be similar and are indicated schematically by the limit flags. Panel (d) shows the fundamental plane rotated about the σ_0 axis and viewed edge-on (for cores). The rotation chosen uses the same power-law combination of r_b and I_b used for the global fundamental plane of elliptical galaxies by Faber *et al.* (1987) and is consistent with their best core plane within the statistical errors. The rms scatter about the central plane (cores only) is 0.12 dex, which is 50% greater than the scatter about the global plane. This increase may be due in part to the influence of central BHs on σ_0 . Five BH candidates from Kormendy & Richstone (1995) are marked in panel (d).

Figure 9: Core versus global properties. Panel (a) plots indicative core magnitude (computed from $L_{core} \equiv \pi r_b^2 I_b$) versus total magnitude. The dashed line is a mean fit assuming unit logarithmic slope (see text). Panel (b) is similar but compares break radius r_b to effective radius r_e . The shaded areas represent predictions of decaying BH binary models (Quinlan & Hernquist 1997).

Figure 10: Inner disk prominence versus ellipticity for power-law galaxies. Disk score (Table 4) is a visual estimate of the evidence for an inner disk: 0 = no evidence, 1 = slight, 2 = probable, 3 = definite. Symbols are the same as for power laws in Fig. 4. Core galaxies are not plotted individually; they lie within the rectangle. If bulges (S0–Sb) are ignored, there is little remaining tendency for power-law galaxies to be highly flattened, as might be expected if they were due to inner disks seen edge-on (Jaffe *et al.* 1994). There is also little tendency for inner disks to appear in flattened galaxies, which would be expected if they were aligned with the outer isophotes. See Appendix B for further discussion.

TABLE 1. Apparent quantities.

Name (1)	Type (2)	Grp (3)	v (4)	Dist (5)	B_T^o (6)	A_B (7)	$(B-V)_o$ (8)	Prof (9)	Nuc (10)	θ_b^{lim} (11)	μ_b^{lim} (12)	θ_b (13)	μ_b (14)	α (15)	β (16)	γ (17)	Src (18)
A 1020	1	0	19500	243.8	15.64	0.20	1.00	\cap		-	-	0.24	17.16	2.56	1.39	0.17	1
A 1831	1	0	22470	280.9	15.08	0.20	1.00	\cap		-	-	0.50	18.70	3.57	1.17	0.11	1
A 2052	1	0	10560	132.0	13.94	0.32	1.00	\cap		-	-	0.42	18.60	8.02	0.75	0.20	1
NGC 221	1	282	64	0.8	8.76	0.31	0.84	\backslash		0.10	11.80	0.14	12.00	0.98	1.36	0.01	4
NGC 221V	1	282	1536	19.2	15.66	0.31	0.84	\backslash		0.05	14.40	2.91	20.65	1.72	3.55	1.21	4
NGC 224	3	282	62	0.8	5.58	0.32	0.95	\cap	++	-	-	0.34	13.68	4.72	0.87	0.12	5
NGC 224V	3	282	1488	18.6	12.48	0.32	0.95	\backslash	+	0.08	14.90	1.91	16.94	4.78	1.05	0.52	5
NGC 524	2	0	1848	23.1	11.31	0.13	1.00	\cap		-	-	0.32	16.12	1.29	1.00	0.00	1
NGC 596	1	26	1696	21.2	11.66	0.12	0.93	\backslash		0.08	14.30	3.50	18.12	0.76	1.97	0.55	1
NGC 720	1	0	1808	22.6	11.16	0.00	1.01	\cap		-	-	3.21	17.50	2.32	1.66	0.06	1
NGC 1023	2	0	816	10.2	10.83	0.25	0.93	\backslash	+	0.05	13.00	1.86	16.36	4.72	1.18	0.78	1
NGC 1172	1	29	2386	29.8	12.55	0.10	0.92	\backslash		0.05	14.10	2.43	18.69	1.52	1.64	1.01	1
NGC 1316	3	31	1428	17.9	9.40	0.00	0.96	\cap		-	-	0.41	14.43	1.16	1.00	0.00	8
NGC 1331	4	31	1723	21.5	14.14	0.04	0.86	\backslash	++	0.05	16.10	4.08	19.98	4.47	1.62	0.67	1
NGC 1399	1	31	1428	17.9	10.55	0.00	1.00	\cap		-	-	3.14	17.06	1.50	1.68	0.07	1
NGC 1400	1	32	1723	21.5	11.62	0.13	1.01	\cap		-	-	0.33	15.51	1.39	1.32	0.00	1
NGC 1426	1	32	1723	21.5	12.25	0.02	0.93	\backslash		0.05	14.05	1.64	17.54	3.62	1.35	0.85	1
NGC 1600	1	34	4019	50.2	11.79	0.08	0.98	\cap		-	-	3.12	18.44	1.98	1.50	0.08	2
NGC 1700	1	100	2840	35.5	12.01	0.12	0.91	\backslash		0.08	13.80	0.09	14.04	0.90	1.30	0.00	1
NGC 2636	1	283	2683	33.5	14.65	0.04	0.88	\backslash		0.10	15.80	0.09	15.71	1.84	1.14	0.04	1
NGC 2832	1	41	7212	90.2	12.80	0.00	0.98	\cap		-	-	0.91	17.45	1.84	1.40	0.02	1
NGC 2841	3	0	1057	13.2	11.64	0.00	0.90	\backslash		0.10	14.40	0.13	14.55	0.93	1.02	0.01	1
NGC 3115	2	0	672	8.4	9.84	0.10	0.97	\backslash	+	0.05	12.45	2.91	16.25	1.47	1.43	0.78	1
NGC 3377	1	57	795	9.9	11.13	0.06	0.84	\backslash		0.05	12.30	0.09	12.90	1.92	1.33	0.29	1
NGC 3379	1	57	795	9.9	10.43	0.05	0.99	\backslash		-	-	1.74	16.14	1.59	1.43	0.18	2
NGC 3384	2	57	795	9.9	11.37	0.05	0.91	\backslash	+	0.08	13.30	-	-	-	-	-	3
NGC 3599	2	48	1624	20.3	12.69	0.00	0.86	\backslash	++	0.05	14.15	1.35	17.58	13.01	1.66	0.79	1
NGC 3605	1	48	1624	20.3	13.24	0.00	0.85	\backslash		0.08	15.30	0.89	17.25	9.14	1.26	0.67	1
NGC 3608	1	48	1624	20.3	11.68	0.00	0.98	\cap		-	-	0.28	15.45	1.05	1.33	0.00	1
NGC 4168	1	0	2914	36.4	11.95	0.04	0.90	\cap		-	-	2.52	18.36	0.95	1.50	0.14	10
NGC 4239	4	56	1224	15.3	13.65	0.07	0.87	\backslash	++	0.05	15.75	1.28	18.42	14.53	0.96	0.65	1
NGC 4365	1	56	1760	22.0	10.64	0.00	0.99	\cap		-	-	1.67	16.77	2.06	1.27	0.15	11
NGC 4387	1	56	1224	15.3	12.87	0.13	0.83	\backslash	+	0.08	15.05	4.42	18.99	3.36	1.59	0.72	1
NGC 4434	1	56	1224	15.3	12.83	0.00	0.87	\backslash		0.05	14.25	2.40	18.21	0.98	1.78	0.70	1
NGC 4458	1	56	1224	15.3	12.78	0.07	0.84	\backslash		0.10	14.40	0.12	14.54	5.26	1.43	0.49	1
NGC 4464	1	56	1224	15.3	13.61	0.00	0.92	\backslash		0.05	13.85	1.21	17.35	1.64	1.68	0.88	1
NGC 4467	1	56	1224	15.3	14.81	0.00	0.93	\backslash		0.05	15.35	3.24	19.98	7.52	2.13	0.98	1
NGC 4472	1	56	1224	15.3	9.32	0.00	0.97	\cap		-	-	2.41	16.66	2.08	1.17	0.04	2
NGC 4478	1	56	1224	15.3	12.14	0.08	0.86	\backslash		0.10	15.15	0.17	15.46	3.32	0.84	0.43	10
NGC 4486	1	56	1224	15.3	9.52	0.08	0.98	\backslash		-	-	7.61	17.92	2.82	1.39	0.25	6
NGC 4486B	1	56	1224	15.3	14.31	0.08	0.96	\cap		-	-	0.18	14.98	2.78	1.33	0.14	1
NGC 4551	1	56	1224	15.3	12.72	0.12	0.90	\backslash	+	0.05	14.75	3.86	18.92	2.94	1.23	0.80	1
NGC 4552	1	56	1224	15.3	10.84	0.14	0.97	\cap		-	-	0.65	15.51	1.48	1.30	0.00	2
NGC 4564	1	56	1224	15.3	11.96	0.03	0.98	\backslash		0.08	13.75	0.52	15.72	0.25	1.90	0.05	10
NGC 4570	2	56	1224	15.3	11.80	0.00	0.92	\backslash	+	0.08	13.70	2.82	17.29	3.72	1.49	0.85	10
NGC 4594	3	0	736	9.2	8.94	0.12	0.90	\backslash		0.08	13.50	-	-	-	-	-	3
NGC 4621	1	56	1224	15.3	10.65	0.07	1.00	\backslash		0.08	13.20	2.92	17.25	0.19	1.71	0.50	2
NGC 4636	1	56	1224	15.3	10.20	0.01	0.95	\backslash		-	-	3.21	17.73	1.64	1.33	0.13	1
NGC 4649	1	56	1224	15.3	9.77	0.03	0.99	\cap		-	-	3.58	17.19	2.00	1.30	0.15	2
NGC 4697	1	0	840	10.5	10.03	0.04	0.95	\backslash	+	0.05	13.55	2.58	16.96	24.86	1.04	0.74	1
NGC 4742	2	0	1000	12.5	12.03	0.09	0.78	\backslash	+	0.05	12.75	1.39	16.76	48.60	1.99	1.09	1
NGC 4874	1	61	7461	93.3	12.31	0.05	1.00	\cap		-	-	2.63	19.22	2.33	1.37	0.13	1
NGC 4889	1	61	7461	93.3	12.48	0.05	0.99	\cap		-	-	1.68	18.05	2.61	1.35	0.05	1
NGC 5813	1	70	2264	28.3	11.39	0.15	0.94	\cap		-	-	0.79	16.53	2.15	1.33	0.08	1
NGC 5845	1	70	2257	28.2	13.35	0.14	0.97	\backslash		0.05	13.75	2.27	17.62	1.27	2.74	0.51	1
NGC 6166	1	73	8997	112.5	12.76	0.00	0.97	\backslash		-	-	2.22	19.35	3.32	0.99	0.08	1
NGC 7332	2	0	1624	20.3	12.50	0.11	0.87	\backslash		0.05	12.90	0.77	15.80	4.25	1.34	0.90	1
NGC 7457	2	0	1089	13.6	12.93	0.21	0.83	\backslash	+	0.05	13.85	-	-	-	-	-	7
NGC 7768	1	234	8251	103.1	12.97	0.13	0.83	\cap		-	-	0.40	17.09	1.92	1.21	0.00	9
VCC 1199	1	56	1224	15.3	16.48	0.05	0.80	\backslash	+	0.05	15.50	1.50	19.68	7.99	1.62	1.13	1
VCC 1440	1	56	1224	15.3	14.82	0.05	0.80	\backslash	+	0.05	15.65	2.52	1	5.54	1.58	0.96	1
VCC 1545	4	56	1224	15.3	14.57	0.05	0.80	\backslash	+	0.05	17.10	1.21	19.71	7.65	1.02	0.62	1
VCC 1627	1	56	1224	15.3	15.64	0.05	0.80	\backslash		0.05	15.35	2.99	20.15	2.12	2.10	0.95	1

Fig. 1: Inner Profiles of 55 Ellipticals and Bulges

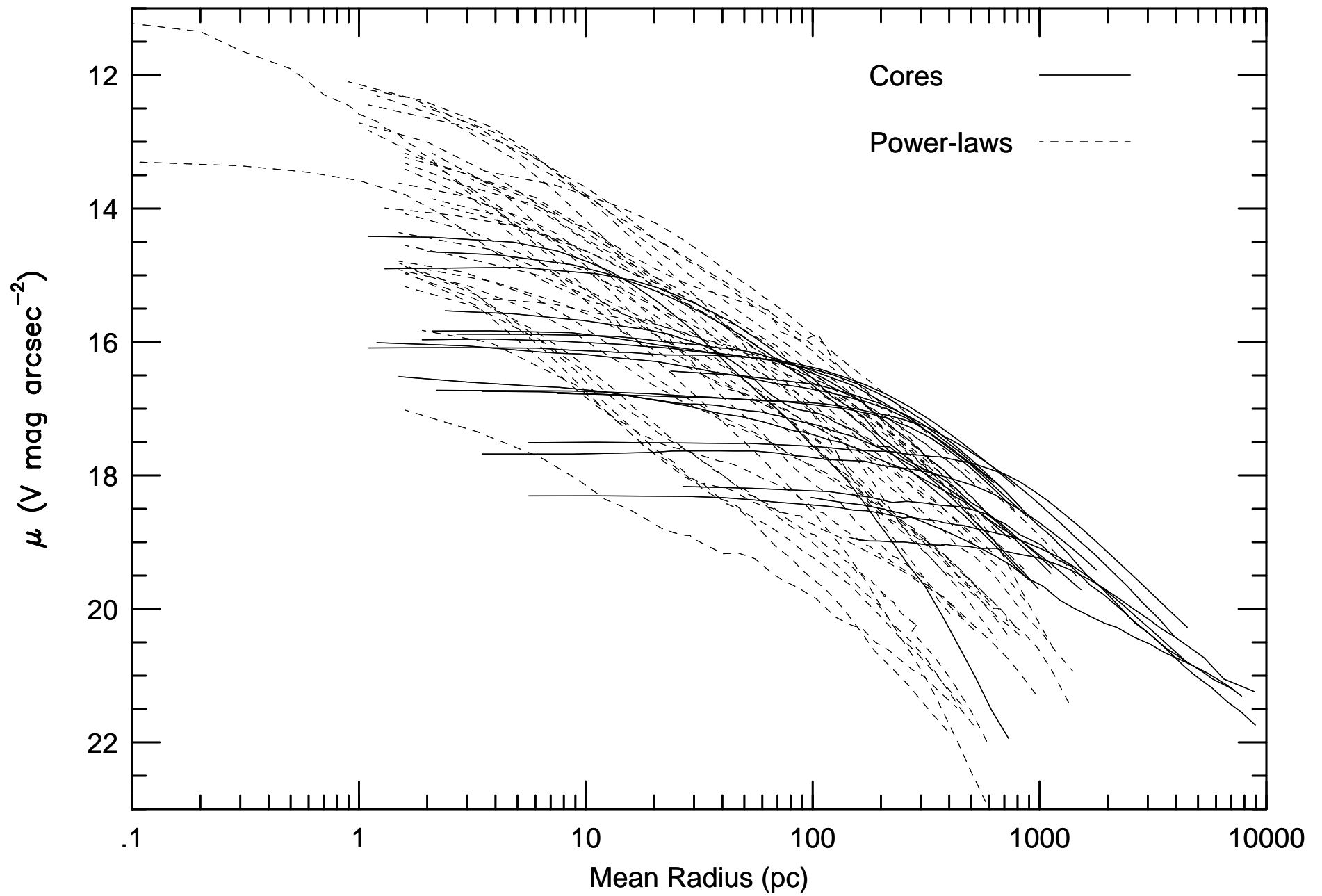


TABLE 2. Absolute quantities.

Name (1)	Type (2)	M_V (3)	σ_0 (4)	R_σ (5)	$(v/\sigma)_*$ (6)	a_4/a (7)	ϵ (8)	Prf (9)	$\log r_b^{lim}$ (10)	μ_b^{lim} (11)	$\log r_b$ (12)	μ_b (13)	α (14)	β (15)	γ (16)	$\log r_e$ (17)	μ_e (18)
A 1020	1	-22.29	-	-	-	-	0.10	\cap	-	-	2.45	17.01	2.56	1.39	0.17	-	-
A 1831	1	-23.16	-	-	-	-	0.15	\cap	-	-	2.83	18.55	3.57	1.17	0.11	-	-
A 2052	1	-22.66	2.398	1.00	-	-	0.24	\cap	-	-	2.43	18.36	8.02	0.75	0.20	-	-
NGC 221	1	-16.60	1.929	1.49	0.89	0.00	0.29	\backslash	-0.40	11.57	-0.26	11.77	0.98	1.36	0.01	2.18	17.85
NGC 221V	1	-16.60	1.740	-	0.89	0.00	0.29	\backslash	0.67	14.17	2.43	20.42	1.72	3.55	1.21	2.18	17.85
NGC 224	3	-19.82	2.342	1.50	0.78	-	0.18	\cap	-	-	0.11	13.44	4.72	0.87	0.12	-	-
NGC 224V	3	-19.82	2.204	-	0.78	-	0.18	\backslash	0.86	14.66	2.24	16.70	4.78	1.05	0.52	-	-
NGC 524	2	-21.51	2.439	-	-	-	0.02	\backslash	-	-	1.55	16.02	1.29	1.00	0.00	-	-
NGC 596	1	-20.90	2.217	-	0.67	1.30	0.20	\backslash	0.92	14.21	2.56	18.03	0.76	1.97	0.55	3.49	20.11
NGC 720	1	-21.62	2.398	1.16	0.32	0.35	0.40	\cap	-	-	2.55	17.50	2.32	1.66	0.06	3.64	20.13
NGC 1023	2	-20.14	2.336	-	-	-	0.62	\backslash	0.39	12.81	1.96	16.17	4.72	1.18	0.78	-	-
NGC 1172	1	-20.74	2.053	-	-	-	0.09	\backslash	0.86	14.03	2.55	18.61	1.52	1.64	1.01	3.75	21.56
NGC 1316	3	-22.82	2.380	1.16	0.91	1.00	0.34	\cap	-	-	1.55	14.43	1.16	1.00	0.00	3.84	19.97
NGC 1331	4	-18.39	-	-	-	-	0.13	\backslash	0.72	16.07	2.63	19.95	4.47	1.62	0.67	3.09	20.57
NGC 1399	1	-21.71	2.522	1.31	0.25	0.10	0.10	\cap	-	-	2.43	17.06	1.50	1.68	0.07	3.56	19.68
NGC 1400	1	-21.06	2.423	-	-	0.00	0.10	\cap	-	-	1.54	15.41	1.39	1.32	0.00	3.60	20.49
NGC 1426	1	-20.35	2.176	-	-	0.00	0.40	\backslash	0.72	14.03	2.23	17.53	3.62	1.35	0.85	3.44	20.40
NGC 1600	1	-22.70	2.531	1.26	0.03	-0.75	0.32	\cap	-	-	2.88	18.38	1.98	1.50	0.08	4.06	21.19
NGC 1700	1	-21.65	2.362	0.98	0.59	0.70	0.28	\backslash	1.14	13.71	1.19	13.95	0.90	1.30	0.00	3.61	19.91
NGC 2636	1	-18.86	1.931	-	-	-	0.05	\backslash	1.21	15.77	1.17	15.68	1.84	1.14	0.04	2.86	18.96
NGC 2832	1	-22.95	2.519	1.22	0.12	-0.30	0.30	\cap	-	-	2.60	17.45	1.84	1.40	0.02	-	-
NGC 2841	3	-19.86	2.360	-	-	-	0.53	\backslash	0.81	14.40	0.92	14.55	0.93	1.02	0.01	-	-
NGC 3115	2	-20.75	2.447	1.80	1.25	-	0.61	\backslash	0.31	12.38	2.07	16.17	1.47	1.43	0.78	3.17	18.76
NGC 3377	1	-19.70	2.182	1.67	0.86	1.05	0.47	\backslash	0.38	12.26	0.64	12.85	1.92	1.33	0.29	3.21	19.92
NGC 3379	1	-20.55	2.352	1.25	0.72	0.10	0.09	\cap	-	-	1.92	16.10	1.59	1.43	0.18	3.23	19.17
NGC 3384	2	-19.53	2.215	-	-	-	0.55	\backslash	0.59	13.26	-	-	-	-	-	-	-
NGC 3599	2	-19.71	1.903	-	-	-	0.21	\backslash	0.69	14.15	2.12	17.58	13.01	1.66	0.79	3.47	21.21
NGC 3605	1	-19.15	2.013	1.06	0.74	-0.80	0.38	\backslash	0.90	15.30	1.94	17.25	9.14	1.26	0.67	3.23	20.57
NGC 3608	1	-20.84	2.290	1.20	0.27	-0.20	0.21	\cap	-	-	1.44	15.45	1.05	1.33	0.00	3.54	20.43
NGC 4168	1	-21.76	2.267	1.05	0.22	0.37	0.09	\cap	-	-	2.65	18.33	0.95	1.50	0.14	3.90	21.33
NGC 4239	4	-18.14	1.778	-	-	-	0.46	\backslash	0.57	15.70	1.98	18.37	14.53	0.96	0.65	3.08	20.74
NGC 4365	1	-22.06	2.418	1.11	0.08	-0.95	0.24	\cap	-	-	2.25	16.77	2.06	1.27	0.15	3.79	20.43
NGC 4387	1	-18.88	2.021	1.10	0.70	-0.75	0.38	\backslash	0.77	14.95	2.52	18.89	3.36	1.59	0.72	3.06	19.97
NGC 4434	1	-18.96	2.061	-	-	-	0.05	\backslash	0.57	14.25	2.25	18.21	0.98	1.78	0.70	3.14	20.29
NGC 4458	1	-18.98	2.021	-	-	-	0.21	\backslash	0.87	14.35	0.95	14.49	5.26	1.43	0.49	3.30	21.07
NGC 4464	1	-18.23	2.097	-	-	-	0.29	\backslash	0.57	13.85	1.95	17.35	1.64	1.68	0.88	2.60	18.32
NGC 4467	1	-17.04	1.857	-	0.61	-	0.24	\backslash	0.57	15.35	2.38	19.98	7.52	2.13	0.98	-	-
NGC 4472	1	-22.57	2.477	1.04	0.43	-0.25	0.17	\cap	-	-	2.25	16.66	2.08	1.17	0.04	3.89	20.43
NGC 4478	1	-19.64	2.130	1.03	0.84	-0.75	0.17	\backslash	0.87	15.09	1.10	15.40	3.32	0.84	0.43	3.02	19.01
NGC 4486	1	-22.38	2.556	1.15	0.11	0.00	0.07	\cap	-	-	2.75	17.86	2.82	1.39	0.25	3.89	20.62
NGC 4486B	1	-17.57	2.301	1.89	0.88	-	0.09	\cap	-	-	1.13	14.92	2.78	1.33	0.14	-	-
NGC 4551	1	-19.10	2.083	1.00	0.55	-0.65	0.26	\backslash	0.57	14.66	2.46	18.83	2.94	1.23	0.80	3.12	20.05
NGC 4552	1	-21.05	2.415	1.16	0.28	0.01	0.06	\cap	-	-	1.68	15.41	1.48	1.30	0.00	3.35	19.25
NGC 4564	1	-19.94	2.217	1.62	1.05	1.00	0.55	\backslash	0.77	13.73	1.59	15.70	0.25	1.90	0.05	3.21	19.66
NGC 4570	2	-20.04	2.290	-	-	1.08	0.70	\backslash	0.77	13.70	2.32	17.29	3.72	1.49	0.85	-	-
NGC 4594	3	-21.78	2.412	1.19	0.89	1.02	0.32	\backslash	0.55	13.41	-	-	-	-	-	-	-
NGC 4621	1	-21.27	2.398	1.22	0.74	1.50	0.34	\backslash	0.77	13.15	2.34	17.20	0.19	1.71	0.50	3.54	19.98
NGC 4636	1	-21.67	2.322	1.05	0.19	-0.10	0.19	\cap	-	-	2.38	17.72	1.64	1.33	0.13	3.88	21.28
NGC 4649	1	-22.14	2.556	1.20	0.42	-0.35	0.17	\cap	-	-	2.42	17.17	2.00	1.30	0.15	3.74	20.11
NGC 4697	1	-21.03	2.243	1.06	0.71	1.30	0.40	\backslash	0.41	13.52	2.12	16.93	24.86	1.04	0.74	3.58	20.46
NGC 4742	2	-19.23	2.021	2.00	1.62	0.41	0.37	\backslash	0.48	12.68	1.93	16.69	48.60	1.99	1.09	2.85	18.58
NGC 4874	1	-23.54	2.462	1.22	0.22	-0.30	0.09	\cap	-	-	3.08	19.18	2.33	1.37	0.13	4.44	22.24
NGC 4889	1	-23.36	2.544	1.12	0.05	0.01	0.33	\cap	-	-	2.88	18.01	2.61	1.35	0.05	4.15	20.97
NGC 5813	1	-21.81	2.352	1.05	0.51	0.01	0.17	\cap	-	-	2.04	16.42	2.15	1.33	0.08	3.82	20.88
NGC 5845	1	-19.87	2.415	2.36	0.91	0.72	0.30	\backslash	0.84	13.65	2.49	17.52	1.27	2.74	0.51	-	-
NGC 6166	1	-23.47	2.477	1.20	0.08	-	0.28	\cap	-	-	3.08	19.35	3.32	0.99	0.08	4.49	22.57
NGC 7332	2	-19.91	2.114	1.56	0.78	-	0.69	\backslash	0.69	12.82	1.88	15.72	4.25	1.34	0.90	-	-
NGC 7457	2	-18.57	1.756	-	-	0.00	0.46	\backslash	0.52	13.69	-	-	-	-	-	-	-
NGC 7768	1	-22.93	2.462	1.16	0.69	0.00	0.29	\cap	-	-	2.30	16.99	1.92	1.21	0.00	4.18	21.52
VCC 1199	1	-15.24	-	-	-	-	0.00	\backslash	0.57	15.46	2.05	19.64	7.99	1.62	1.13	-	-
VCC 1440	1	-16.90	-	-	-	-	0.00	\backslash	0.57	15.61	2.27	19.95	5.54	1.58	0.96	-	-
VCC 1545	4	-17.15	-	-	-	-	0.10	\backslash	0.57	17.06	1.95	19.67	7.65	1.02	0.62	-	-
VCC 1627	1	-16.08	-	-	-	-	0.05	\backslash	0.57	15.31	2.35	20.11	2.12	2.10	0.95	-	-

Fig. 2: M31 and M32 as Seen Locally and at Virgo

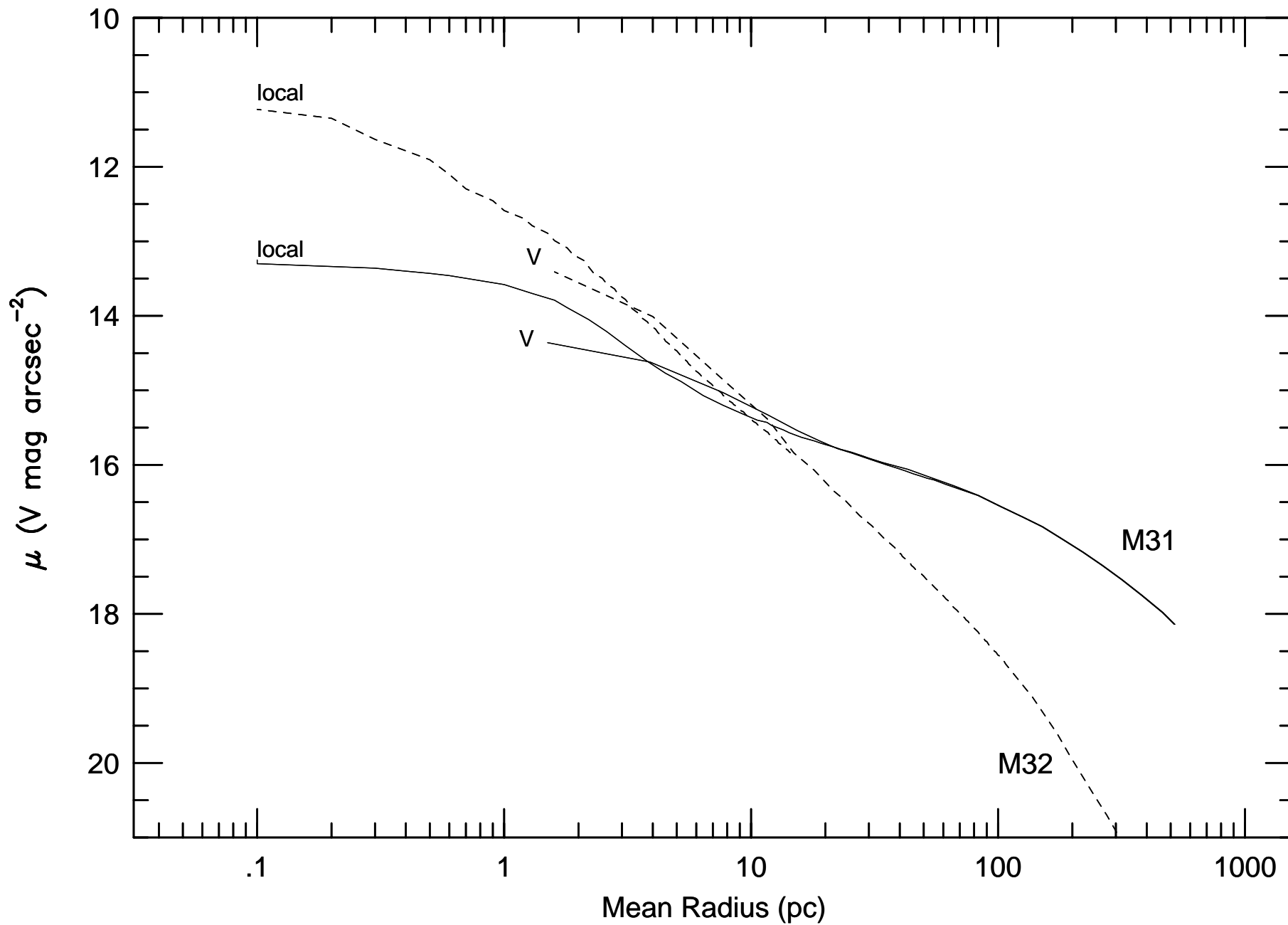


TABLE 3. Local quantities from nuker-law fits.

Name (1)	Type (2)	M_V (3)	Prof (4)	M/L_V (5)	$j(0''.1)$ (6)	$f(0''.1)$ (7)	$L(\leq 0''.1)$ (8)	$M(\leq 0''.1)$ (9)	$\sigma^P(0''.1)$ (10)	$t(0''.1)$ (11)	$r(0''.1)$ (12)	$j(10)$ (13)	$L(\leq 10)$ (14)	$\sigma(10)$ (15)	$t(10)$ (16)
A 1020	1	-22.29	∩	–	1.291+01	–	1.169+08	–	–	–	0.01	1.142+02	7.655+05	–	–
A 1831	1	-23.16	∩	–	1.242+00	–	1.779+07	–	–	–	0.01	1.430+01	9.394+04	–	–
A 2052	1	-22.66	∩	12.8	3.753+00	9.184-07	6.440+06	8.226+07	2.154+02	1.005+14	0.02	3.004+01	2.081+05	6.620+01	1.365+12
NGC 221	1	-16.60	\	2.27	5.412+05	1.897-01	2.024+05	4.603+05	8.046+01	6.892+08	2.58	1.241+03	1.698+07	8.287+01	3.065+11
NGC 221V	1	-16.60	\	1.29	1.467+03	3.795-04	1.878+07	2.424+07	6.460+01	2.614+11	0.11	1.253+03	1.988+07	6.767+01	2.984+11
NGC 224	3	-19.82	∩	26.1	4.783+04	1.634-02	1.441+04	3.756+05	1.983+02	8.131+09	2.66	8.233+02	8.442+06	2.372+02	8.562+11
NGC 224V	3	-19.82	\	3.12	8.330+02	2.403-04	5.176+06	1.613+07	1.255+02	4.233+11	0.11	7.123+02	6.034+06	9.062+01	5.320+11
NGC 524	2	-21.51	∩	14.3	2.236+02	3.146-05	1.543+06	2.200+07	2.369+02	3.173+12	0.09	2.375+02	1.153+06	1.828+02	2.888+12
NGC 596	1	-20.90	\	4.16	1.180+03	1.492-04	1.108+07	4.613+07	1.458+02	6.398+11	0.10	1.232+03	1.064+07	1.272+02	6.052+11
NGC 720	1	-21.62	∩	8.15	2.486+01	3.836-06	1.941+05	1.582+06	2.391+02	3.101+13	0.09	2.679+01	1.601+05	1.444+02	2.619+13
NGC 1023	2	-20.14	\	5.99	6.920+03	5.320-04	8.615+06	5.159+07	1.890+02	1.783+11	0.20	1.980+03	2.036+07	1.853+02	7.630+11
NGC 1172	1	-20.74	\	2.57	9.684+02	9.437-05	3.710+07	9.541+07	1.177+02	9.704+11	0.07	2.030+03	2.574+07	1.189+02	4.744+11
NGC 1316	3	-22.82	∩	2.56	1.209+03	5.416-05	3.911+06	9.997+06	2.059+02	1.936+12	0.12	1.113+03	5.590+06	1.574+02	2.214+12
NGC 1331	4	-18.39	\	–	1.211+02	–	1.302+06	–	–	–	0.10	1.302+02	1.230+06	–	–
NGC 1399	1	-21.71	∩	12.73	8.711+01	9.977-06	3.239+05	4.123+06	3.083+02	1.114+13	0.12	7.854+01	4.454+05	2.011+02	1.395+13
NGC 1400	1	-21.06	∩	10.7	5.418+02	3.758-05	2.997+06	3.207+07	2.433+02	2.596+12	0.10	5.542+02	2.679+06	2.128+02	2.514+12
NGC 1426	1	-20.35	\	4.91	1.148+03	1.595-04	1.427+07	7.007+07	1.389+02	5.845+11	0.10	1.244+03	1.358+07	1.305+02	5.355+11
NGC 1600	1	-22.70	∩	14.3	6.870+00	1.172-06	6.016+05	8.582+06	3.032+02	9.039+13	0.04	1.569+01	9.933+04	1.178+02	1.381+13
NGC 1700	1	-21.65	\	4.00	1.351+03	3.886-05	4.849+07	1.938+08	2.202+02	2.267+12	0.06	2.750+03	1.743+07	1.892+02	9.049+11
NGC 2636	1	-18.86	\	2.97	2.910+02	1.239-04	7.509+06	2.228+07	8.088+01	8.046+11	0.06	4.787+02	2.514+06	7.231+01	4.480+11
NGC 2832	1	-22.95	∩	10.9	8.366+00	2.659-07	3.239+06	3.522+07	3.169+02	3.648+14	0.02	1.400+01	7.344+04	2.187+02	1.355+14
NGC 2841	3	-19.86	\	8.98	1.944+03	2.580-04	3.180+06	2.854+07	1.949+02	3.807+11	0.16	1.128+03	7.568+06	1.775+02	8.125+11
NGC 3115	2	-20.75	\	7.14	1.589+04	5.798-04	1.112+07	7.942+07	2.517+02	1.596+11	0.25	3.216+03	3.314+07	2.555+02	9.963+11
NGC 3377	1	-19.70	\	2.88	1.538+04	8.367-04	1.254+07	3.610+07	1.511+02	1.158+11	0.21	4.090+03	3.838+07	1.541+02	4.445+11
NGC 3379	1	-20.55	∩	6.87	7.770+02	1.860-04	5.594+05	3.841+06	1.909+02	6.007+11	0.21	3.918+02	2.406+06	1.567+02	2.289+12
NGC 3599	2	-19.71	\	2.09	7.588+02	3.425-04	7.502+06	1.564+07	7.275+01	2.976+11	0.10	7.375+02	7.649+06	6.657+01	3.075+11
NGC 3605	1	-19.15	\	4.05	5.053+02	2.619-04	4.536+06	1.835+07	9.195+01	3.853+11	0.10	4.921+02	4.634+06	7.937+01	3.987+11
NGC 3608	1	-20.84	∩	7.04	7.031+02	9.023-05	3.680+06	2.589+07	1.755+02	1.095+12	0.10	6.936+02	3.816+06	1.520+02	1.117+12
NGC 4168	1	-21.76	∩	7.54	4.032+01	2.029-05	1.360+06	1.026+07	1.572+02	5.160+12	0.06	6.862+01	4.280+05	8.059+01	1.801+12
NGC 4239	4	-18.14	\	3.37	2.744+02	9.189-04	1.041+06	3.506+06	4.907+01	1.224+11	0.13	1.678+02	1.560+06	4.228+01	2.304+11
NGC 4365	1	-22.06	∩	8.40	1.198+02	2.174-05	9.292+05	7.810+06	2.352+02	4.900+12	0.09	1.276+02	8.188+05	1.395+02	4.282+12
NGC 4387	1	-18.88	\	5.34	6.272+02	5.281-04	2.512+06	1.343+07	8.642+01	1.949+11	0.13	3.754+02	3.683+06	7.718+01	3.626+11
NGC 4434	1	-18.96	\	4.73	1.271+03	4.039-04	4.985+06	2.357+07	1.064+02	2.460+11	0.13	7.662+02	7.366+06	1.021+02	4.485+11
NGC 4458	1	-18.98	\	4.00	2.816+03	4.420-04	7.837+06	3.134+07	1.138+02	2.210+11	0.13	1.882+03	1.350+07	1.139+02	2.921+11
NGC 4464	1	-18.23	\	4.82	2.088+03	3.382-04	9.495+06	4.578+07	1.263+02	2.824+11	0.13	1.197+03	1.330+07	1.259+02	5.104+11
NGC 4467	1	-17.04	\	6.27	5.270+02	6.063-04	2.649+06	1.662+07	7.082+01	1.675+11	0.13	2.918+02	3.593+06	7.048+01	3.002+11
NGC 4472	1	-22.57	∩	9.20	5.510+01	4.885-06	1.253+05	1.152+06	2.842+02	2.493+13	0.13	4.594+01	2.483+05	2.046+02	3.701+13
NGC 4478	1	-19.64	\	5.03	9.574+02	3.294-04	2.863+06	1.439+07	1.132+02	3.111+11	0.13	6.657+02	4.802+06	1.017+02	4.911+11
NGC 4486	1	-22.38	∩	17.7	1.491+02	1.310-04	4.354+05	7.690+06	2.919+02	8.139+11	0.13	1.030+02	7.360+05	1.234+02	1.677+12
NGC 4486B	1	-17.57	∩	9.85	1.405+03	1.536-04	2.977+06	2.933+07	1.814+02	6.385+11	0.13	1.144+03	6.097+06	1.796+02	7.609+11
NGC 4551	1	-19.10	\	7.25	8.060+02	4.281-04	3.444+06	2.498+07	1.050+02	2.313+11	0.13	4.709+02	4.929+06	9.835+01	4.251+11
NGC 4552	1	-21.05	∩	7.66	4.634+02	2.678-05	8.494+05	6.510+06	2.403+02	4.027+12	0.13	4.241+02	1.944+06	2.089+02	4.520+12
NGC 4564	1	-19.94	\	4.78	3.041+03	2.939-04	1.123+07	5.365+07	1.554+02	3.220+11	0.13	1.825+03	1.692+07	1.514+02	5.795+11
NGC 4570	2	-20.04	\	5.52	3.255+03	2.504-04	1.451+07	8.011+07	1.768+02	3.693+11	0.13	1.874+03	2.046+07	1.698+02	6.759+11
NGC 4621	1	-21.27	\	6.73	5.920+03	1.833-04	2.611+07	1.757+08	2.452+02	4.830+11	0.13	3.370+03	3.687+07	2.434+02	8.706+11
NGC 4636	1	-21.67	∩	10.4	7.270+01	5.512-05	1.890+05	1.974+06	1.871+02	2.124+12	0.13	5.462+01	3.423+05	1.082+02	3.932+12
NGC 4649	1	-22.14	∩	16.2	1.252+02	4.113-05	3.370+05	5.454+06	3.135+02	2.653+12	0.13	9.153+01	5.972+05	1.673+02	5.233+12
NGC 4697	1	-21.03	\	6.78	3.468+03	6.311-04	4.562+06	3.093+07	1.535+02	1.549+11	0.20	1.072+03	1.068+07	1.460+02	6.270+11
NGC 4742	2	-19.23	\	1.76	7.615+03	5.447-04	2.339+07	4.117+07	1.132+02	1.764+11	0.17	2.676+03	3.691+07	1.138+02	4.609+11

TABLE 3. Local Quantities from Nuker-law Fits.

Name (1)	Type (2)	M_V (3)	Prof (4)	M/L_V (5)	$j(0''.1)$ (6)	$f(0''.1)$ (7)	$L(\leq 0''.1)$ (8)	$M(\leq 0''.1)$ (9)	$\sigma^P(0''.1)$ (10)	$t(0''.1)$ (11)	$r(0''.1)$ (12)	$j(10)$ (13)	$L(\leq 10)$ (14)	$\sigma(10)$ (15)	$t(10)$ (16)
NGC 4874	1	-23.54	\cap	15.0	2.531+00	8.733-07	1.508+06	2.262+07	2.627+02	1.141+14	0.02	1.270+01	8.464+04	6.811+01	3.160+12
NGC 4889	1	-23.36	\cap	11.2	3.135+00	1.312-07	1.623+06	1.813+07	3.407+02	7.701+14	0.02	1.077+01	6.680+04	1.406+02	4.584+13
NGC 5813	1	-21.81	\cap	7.10	9.256+01	7.622-06	1.296+06	9.206+06	2.133+02	1.383+13	0.07	1.124+02	6.304+05	1.621+02	9.291+12
NGC 5845	1	-19.87	\backslash	6.69	9.091+02	4.600-05	1.906+07	1.275+08	2.364+02	1.959+12	0.07	1.432+03	1.181+07	1.883+02	1.016+12
NGC 6166	1	-23.47	\cap	15.6	8.325-01	2.401-07	8.377+05	1.305+07	2.825+02	4.295+14	0.02	4.576+00	2.967+04	6.675+01	8.591+12
NGC 7332	2	-19.91	\backslash	1.56	3.820+03	1.871-04	4.151+07	6.474+07	1.300+02	5.005+11	0.10	3.706+03	4.225+07	1.266+02	5.168+11
NGC 7768	1	-22.93	\cap	9.51	1.562+01	6.059-07	8.470+06	8.053+07	2.718+02	1.526+14	0.02	1.713+01	7.196+04	2.451+02	1.805+14
VCC 1199	1	-15.24	\backslash	-	5.253+02	-	3.096+06	-	-	-	0.13	2.781+02	4.015+06	-	-
VCC 1440	1	-16.90	\backslash	-	3.795+02	-	1.871+06	-	-	-	0.13	2.114+02	2.553+06	-	-
VCC 1545	4	-17.15	\backslash	-	7.286+01	-	2.703+05	-	-	-	0.13	4.500+01	4.086+05	-	-
VCC 1627	1	-16.08	\backslash	-	5.000+02	-	2.439+06	-	-	-	0.13	2.796+02	3.340+06	-	-

Notes to TABLE 3.

Col. 1: Name (see Table 1).

Col. 2: Hubble type (see Table 1).

Col. 3: Absolute V mag of bulge component from Table 1.

Col. 4: Profile class: \cap = core; \backslash = power law.

Columns 5-11 are based on nuker law fits to the brightness profile from Table 2 (see text). M/L is assumed constant, and the velocity dispersion is isotropic everywhere. The models are mass-normalized by fitting to the central dispersion, σ_0 , assuming that it is measured through a $2'' \times 2''$ aperture (in perfect seeing). If σ_0 is missing, columns 5, 7, 9, 10, 11, 15, and 16 are blank.

Col. 5: Normalized M/L_V in solar units.

Col. 6: $j(0''.1)$ is the luminosity density at a radius of $0''.1$ in $L_\odot \text{ pc}^{-3}$.

Col. 7: Equivalent Maxwellian peak phase-space density at $0''.1$, given by $\rho/(2\pi\sigma^2)^{3/2}$, in units of $M_\odot \text{ pc}^{-3} (\text{km s}^{-1})^{-3}$.

Col. 8: V -band luminosity within a sphere of radius $0''.1$, in L_\odot .

Col. 9: Mass within a sphere of radius $0''.1$, in M_\odot .

Col. 10: Projected line-of-sight velocity dispersion at $0''.1$, in km s^{-1} .

Col. 11: Local relaxation time in yr at a radius of $0''.1$ from Equation (8-71) of Binney and Tremaine (1987). The Coulomb log has been set to $\log(0.4M(\leq 0''.1)/0.7M_\odot)$, where $M(\leq 0''.1)$ is from column 9.

Col. 12: Physical radius corresponding to $0''.1$, in pc.

Col. 13: Luminosity density as in column 5, but at a radius of 10 pc.

Col. 14: Enclosed luminosity as in column 8, but within a sphere of 10 pc.

Col. 15: Radial velocity dispersion at 10 pc (note: not line-of-sight as in column 10).

Col. 16: Local relaxation time as in column 11, but at 10 pc.

Figure 3: Division into Cores and Power-laws

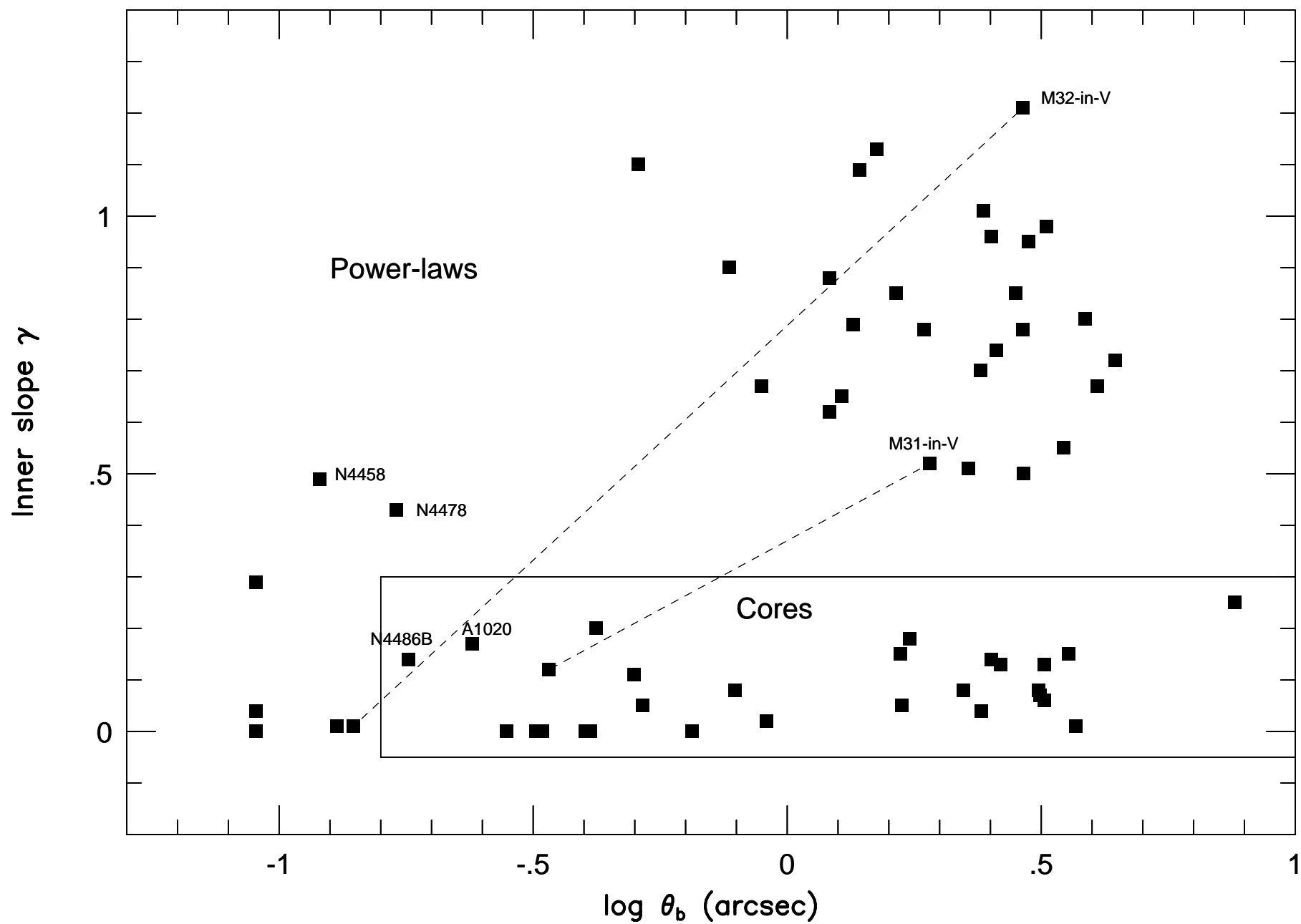


TABLE 4. Inner disk survey of power-law galaxies.

Name	ϵ	Nuc	Disk score	Comments
NGC 221	0.29		0	Smooth SB profile, ellipsoidal and featureless at all radii. No sign of cold disk in kinematic data.
NGC 224	0.18	+	0	Sb galaxy. SB profile complex, but no sign of inner cold disk in kinematic data.
NGC 596	0.20		0	Smooth SB profile, ellipsoidal and featureless at all radii.
NGC 1023	0.62	+	2	S0 galaxy. Ledge in SB profile at $0''.2$ with higher ϵ inside. Peak in a_4 at $0''.5$ suggests disk.
NGC 1172	0.09		0	Smooth SB profile. Quite round. Inner a_4 's boxy, but dust interferes.
NGC 1331	0.13	++	1	Ledge in SB profile at $0''.3$ with ϵ higher inside $0''.1$. a_4 's neutral.
NGC 1426	0.40		0	Smooth SB profile, ellipsoidal and featureless at all radii.
NGC 1700	0.28		0	Smooth SB profile, ellipsoidal and featureless. Inner dust mottling adds uncertainty.
NGC 2636	0.05		0	Smooth SB profile, ellipsoidal and featureless at all radii.
NGC 2841	0.53		3	Sa galaxy. Tilted inner disk with dust arms.
NGC 3115	0.61	+	3	S0 galaxy. Visible edge-on inner disk.
NGC 3377	0.47		1:	Dust perturbs inner a_4 's. Possible dust disk (see text).
NGC 3384	0.55	+	2	S0 galaxy. Cliff in SB profile at $2''$. Weak disk when model subtracted.
NGC 3599	0.21	++	3	Cliff in profile at $2''$. Nearly face-on spiral dust arms inside this radius.
NGC 3605	0.38		1	Weak bump in SB profile at $2''$ marks change from boxy outer to disky inner, but ϵ falls within $2''$. Confused.
NGC 4239	0.46	++	2	Cliff in SB profile at $2''$ with disky a_4 inside. ϵ falls inside $1''$.
NGC 4387	0.38	+	1	Weak ledge in profile at $0''.3$. Weakly disky a_4 inside $1''$.
NGC 4434	0.05		0	Smooth SB profile, ellipsoidal and featureless at all radii.
NGC 4458	0.21	-		Smooth SB profile with incipient core. Probable edge-on inner disk but <i>not</i> a power law.
NGC 4464	0.29		0	Smooth SB profile, ellipsoidal and featureless at all radii.
NGC 4467	0.24		1	Smooth SB profile, ellipsoidal and featureless at all radii, though ϵ is high at $1''$.
NGC 4478	0.17		2	Smooth SB profile. Disk impression strong on direct image but subtracted model shows no residual disk, unlike Jaffe <i>et al.</i>
NGC 4551	0.26	+	1	Smooth SB profile. Subtracted model shows possible residual disk, but a_4 's are neutral.
NGC 4564	0.55		0	Galaxy is globally flattened yet middle is round and featureless.
NGC 4570	0.70	+	3	S0 galaxy. Subtracted model shows thin disk close to edge-on.
NGC 4594	0.32		3	Sa galaxy. Visible inner disk nearly edge-on.
NGC 4621	0.34		3	Inner disk nearly edge-on.
NGC 4697	0.40	+	3	Highly inclined inner dust disk, possibly with some stars.
NGC 4742	0.37	+	2	Cliff in SB profile at $2''$. High ϵ throughout inner galaxy. Dust (ring?) at $0''.5$ confuses a_4 's.
NGC 5845	0.30		3	Visible edge-on inner disk.
NGC 7332	0.69		3	Visible edge-on inner disk, confused by dust mottling.
NGC 7457	0.46	+	-	Early WFPC1 picture not adequate for assessment.
VCC 1199	0.00	+	1	Weak nucleus, otherwise ellipsoidal and featureless at all radii, though ϵ high inside $1''$.
VCC 1440	0.00	+	0	Weak nucleus, otherwise ellipsoidal and featureless at all radii.
VCC 1545	0.10	+	0	Weak nucleus, otherwise ellipsoidal and featureless at all radii.
VCC 1627	0.05		1	Weak nucleus, otherwise ellipsoidal and featureless at all radii, though ϵ moderate inside $1''$.

Inner disk score: 0 = no sign of a disk; 1 = possible disk; 2 = probable disk; and 3 = disk plainly visible.

Fig. 4. Central Parameters vs. Absolute Magnitude

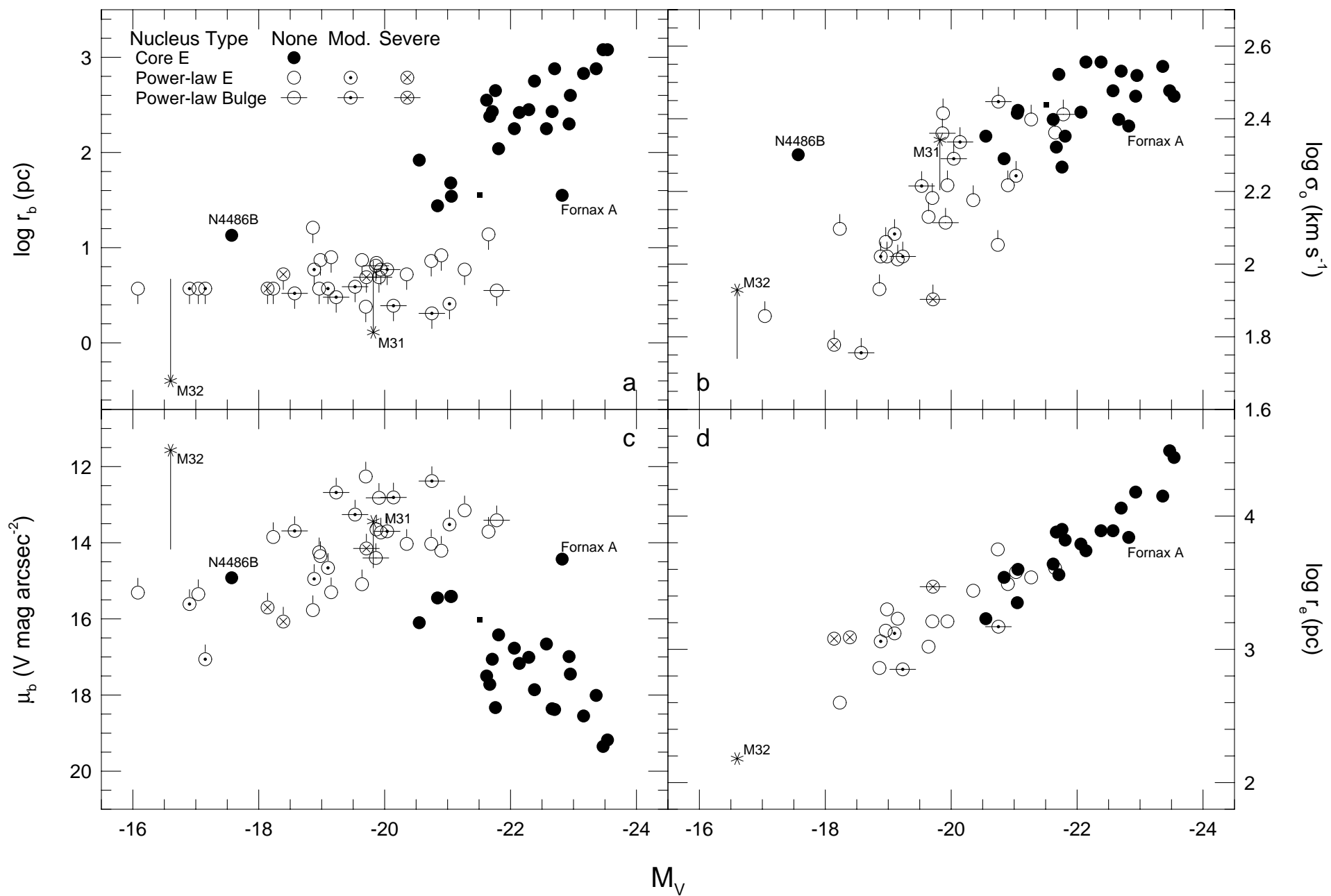


Fig. 5: Cores and Power-Laws vs. Distance

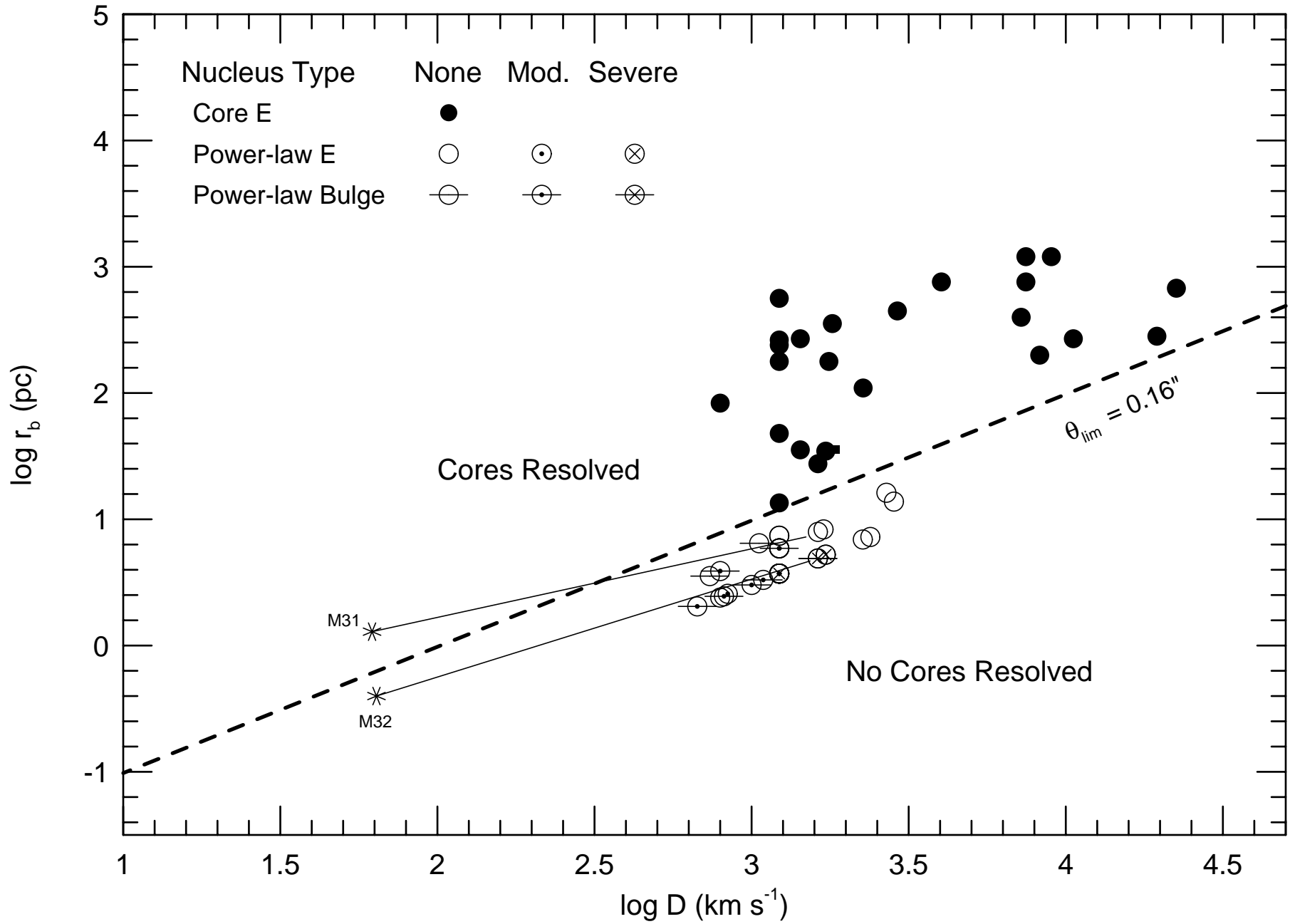


Fig. 6. Densities at 0.1" vs. Absolute Magnitude

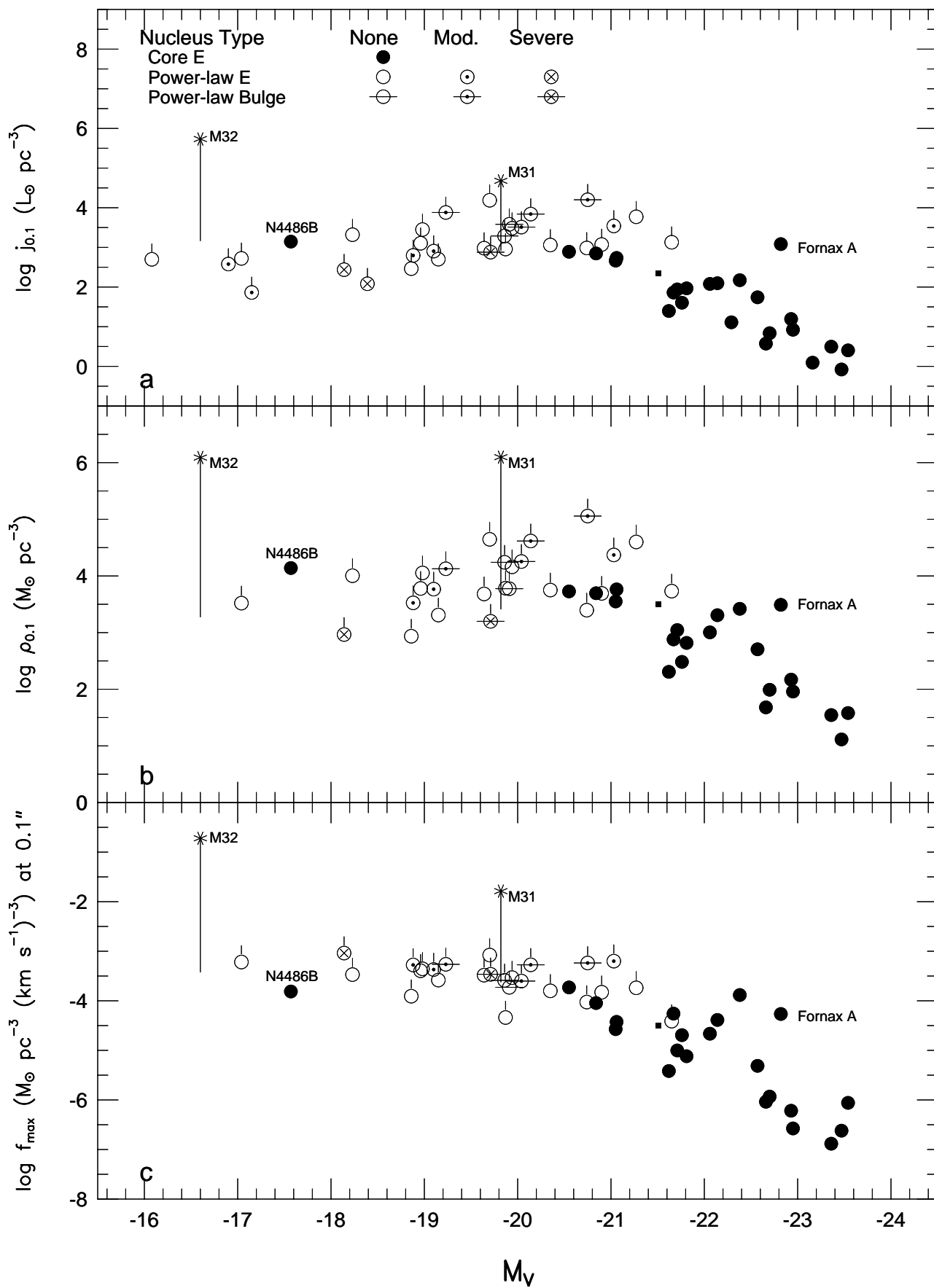


Fig. 7. Correlation with Rotation and Isophote Shape

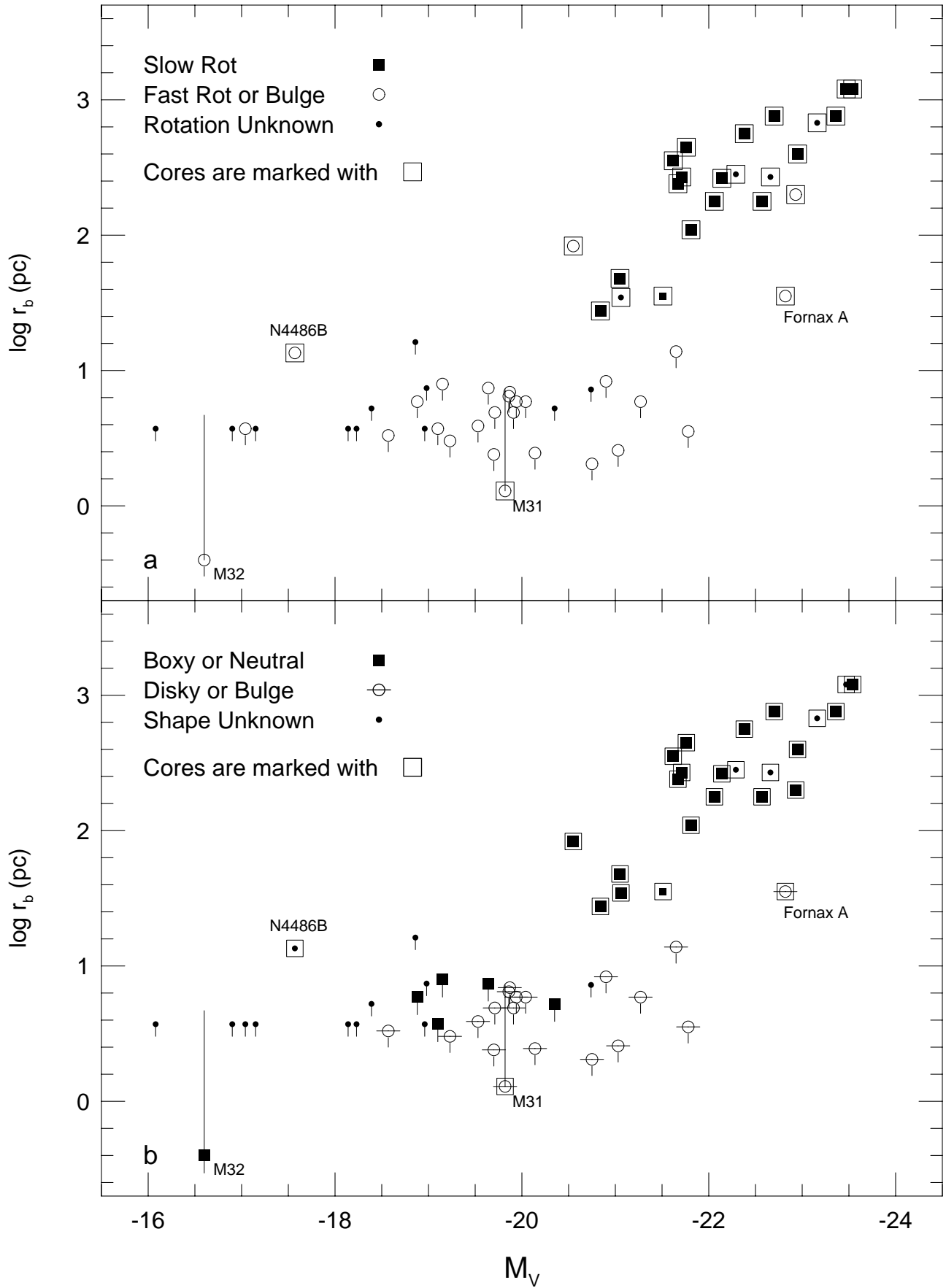


Fig. 8. Projections of the Core Fundamental Plane

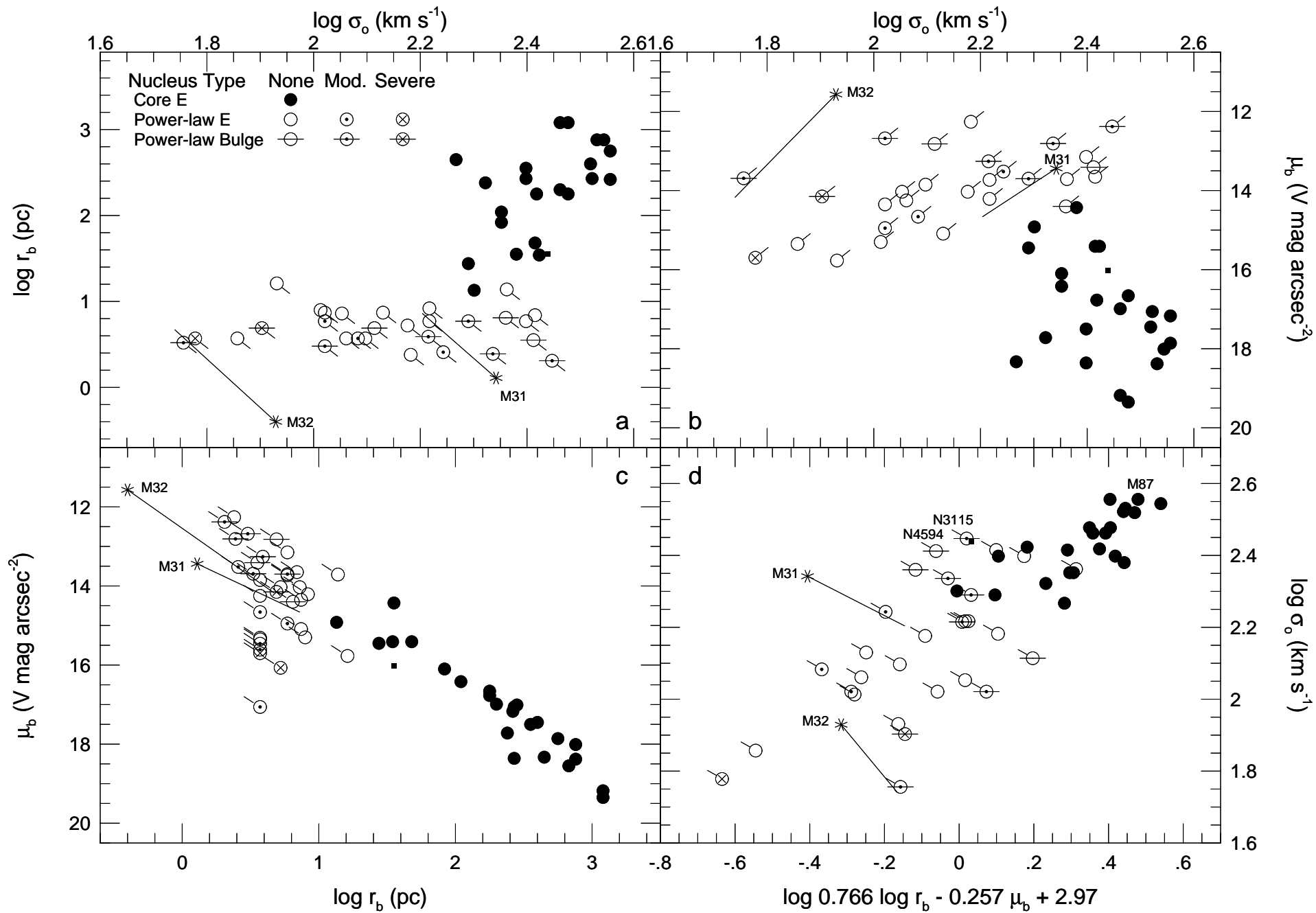


Fig. 9. Core vs. Global Properties

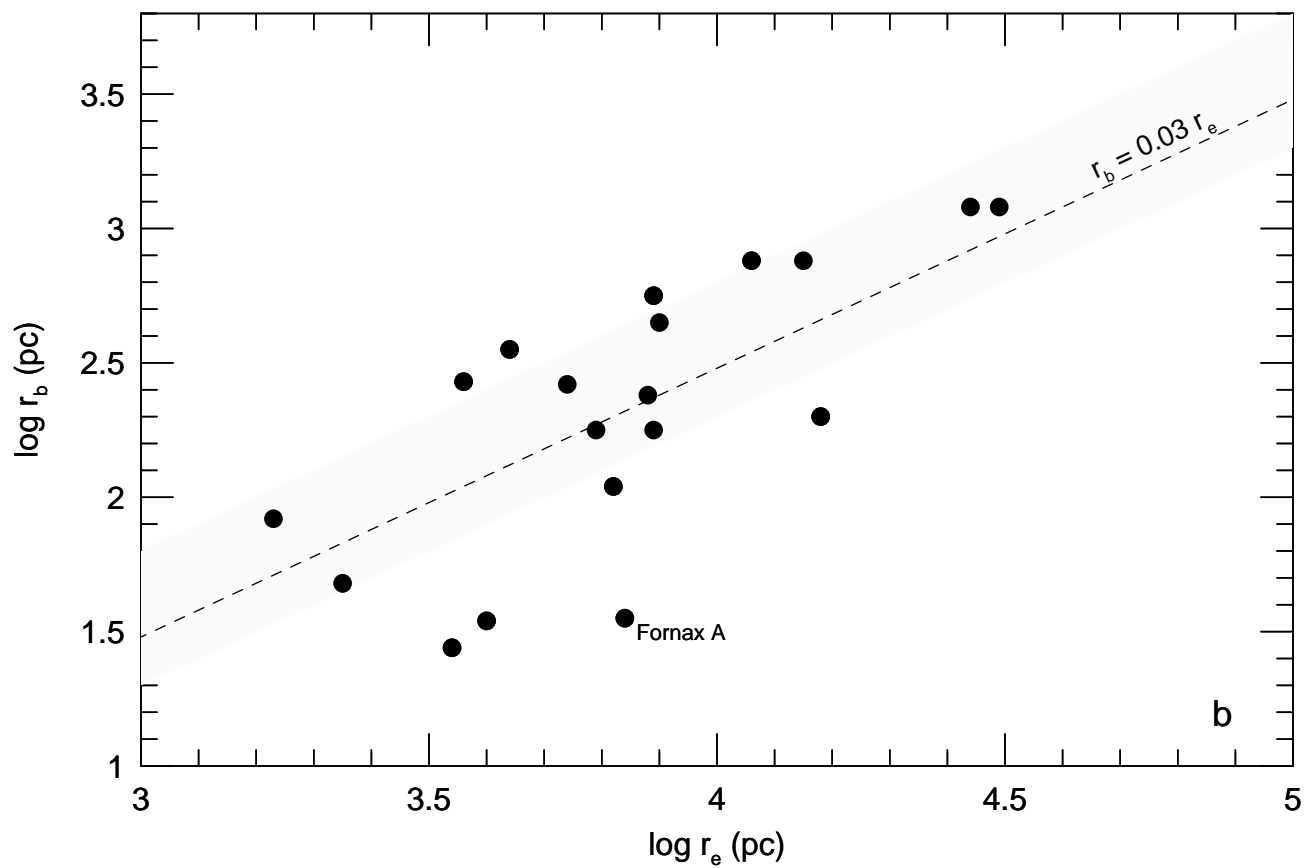
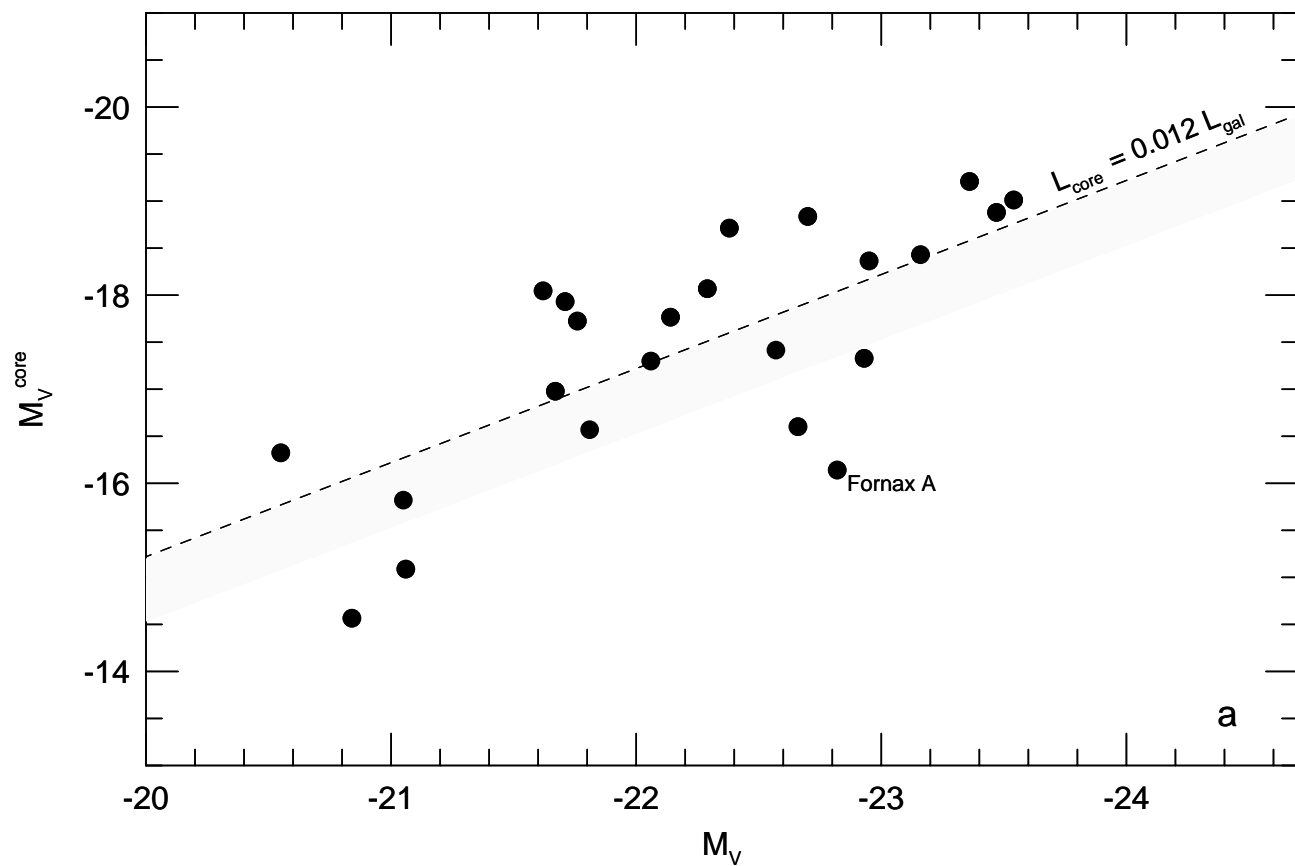
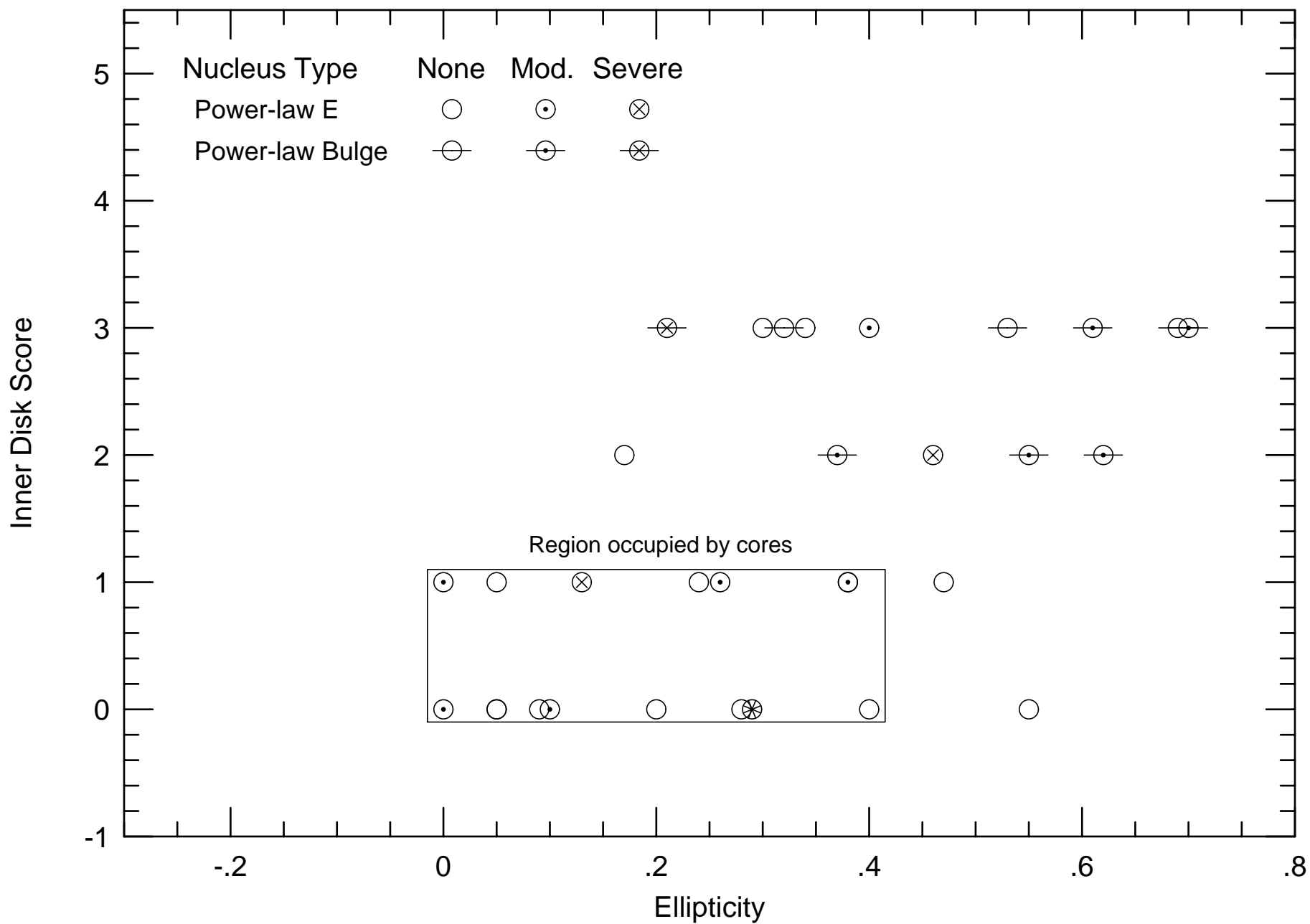


Fig. 10: Inner Disk Prominence vs. Ellipticity for Power-Laws Galaxies



Notes to TABLE 1.

- Col. 1: Name. “A” objects are first-brightest Abell cluster galaxies. “VCC” objects are dwarf Virgo Cluster E’s from Binggeli, Sandage, and Tammann (1985). M 31 = NGC 224; M 32 = NGC 221; M 87 = NGC 4486. The entries for NGC 221 and NGC 224 followed by “V” denote M 31 and M 32 as seen 24 times further away, just beyond the Virgo Cluster.
- Col. 2: Hubble type from the *Second Reference Catalog of Bright Galaxies* (de Vaucouleurs *et al.* 1976, RC2): 1=E, 2=E/S0 or S0, 3=Sa or Sb, 4=dE or dSph.
- Col. 3: Group number from Faber *et al.* (1989).
- Col. 4: Adopted distance in units of km s^{-1} . Group membership information is used where available. The following distance estimates are combined in descending order of weight: 1) Surface-brightness fluctuation method (Tonry, unpublished). 2) $D_n - \sigma$ average for Faber *et al.* (1989) groups with 3 or more members. 3) Radial velocity (group or single) corrected by smooth peculiar velocity field as determined by POTENT (Dekel *et al.*, in preparation). 4) Radial velocity in cosmic microwave background frame (for distant objects).
- Col. 5: Distance in column 4 converted to Mpc using $H_0 = 80 \text{ km s}^{-1} \text{ Mpc}^{-1}$.
- Col. 6: Fully corrected B_T^o of bulge component, from Faber *et al.* (1989) where available (E’s only, magqual ≥ 2), otherwise mostly from the RC2 and/or the *Third Reference Catalog of Bright Galaxies* (de Vaucouleurs *et al.* 1991, RC3). Special sources of magnitudes: VCC ellipticals: Binggeli and Cameron (1993); Bender (priv. comm.). Abell brightest cluster galaxies (BCGs): add 0.21 mag to VI mag of Hoessel *et al.* (1980), where the constant is determined from 7 galaxies with VI and B_T^o in common.
- Bulge/total brightness ratios (in B-band) for S0’s and spirals: NCG 224 = 0.24 from de Vaucouleurs (1958). NGC 524 = 0.88 and NGC 1023 = 0.51 from Kormendy and Illingworth (1983). NGC 2814 = 0.24 from Boroson (1981). NCG 3115 = 0.94 from Capaccioli *et al.* (1987). NGC 3384 = 0.59 from Burstein (1979). NGC 4594 = 0.93 from Burkhead (1986). NGC 7332 = 0.58 from average of S0’s in Simien and de Vaucouleurs (1986). NGC 7457 = 0.38 from Burstein (1979) and Kormendy (1977).
- Col. 7: B-band Galactic extinction A_B from Faber *et al.* (1989) or RC3.
- Col. 8: Fully corrected $(B - V)_o$ from Faber *et al.* (1989) where available, otherwise from RC3. Bulge $(B - V)_o$ for some S0-Sb’s is a guess.
- Col. 9: Profile class: \cap = core; \setminus = power law.
- Col. 10: Degree of nucleation: ++ = severe, + = moderate. M 31-in-Virgo is the dividing line between severe and moderate (see Figure 2).
- Col. 11: Upper limit to break θ_b (in arcsec) for power-law galaxies only. Based on simulated model profiles convolved with HST PSF and then deconvolved to match data. Most values are from Paper I, but some are new here. Used in preference to θ_b for power-law galaxies, see text.
- Col. 12: Lower limit to break surface brightness μ_b , for power law galaxies only. Goes with θ_b^{lim} in column 11. Raw value uncorrected for Galactic extinction in V mag arcsec $^{-2}$. Most values are from Paper I, but some are new here. Used in preference to μ_b for power-law galaxies, see text.
- Col. 13: Break radius θ_b in arcsec from nuker-law fit. Most fits are from Paper II, but some are new here. Used for core galaxies, see text.
- Col. 14: Break surface brightness μ_b in V mag arcsec $^{-2}$ from nuker-law fit. Raw value uncorrected for Galactic extinction, in V mag arcsec $^{-2}$. Used for core galaxies, see text.
- Col. 15-17: α , β , and γ from nuker-law fit, mostly from Paper II.
- Col. 18: Sources of HST images: 1 = Paper I; 2 = WFPC1 Team GTO program (Ajhar *et al.*, in preparation); 3 = WFPC1 Team GTO program, unpublished; 4 = Lauer *et al.* (1992a); 5 = Lauer *et al.* (1993); 6 = Lauer *et al.* (1992b); 7 = Lauer *et al.* (1991); 8 = Shaya *et al.* (1996); 9 = Grillmair *et al.* (1994); 10 = Jaffe *et al.* (1994; Virgo survey); 11 = Forbes *et al.* (1995; kinematically decoupled cores).

Notes to TABLE 2.

- Col. 1: Name (see Table 1).
- Col. 2: Hubble type (see Table 1).
- Col. 3: Absolute V mag of bulge component based on B_T^o , $(B - V)_o$, and distance from Table 1 ($H_0 = 80 \text{ km s}^{-1} \text{ Mpc}^{-1}$). No K-correction or cosmological corrections have been applied.
- Col. 4-5: Logarithm of central velocity dispersion, σ_0 , and ratio of central dispersion to projected dispersion at $10''$, σ_0/σ_{10} . The geometric mean of σ_{10} on major and minor axes is used if both are available. σ_0 is assumed to equal to the rms luminosity-weighted value through a $2'' \times 2''$ aperture in $1''$ FWHM seeing. Quoted values are weighted means from the following sources: Bender & Nieto (1990); Bender *et al.* (1994); Bertola *et al.* (1988); Binney *et al.* (1990); Davies & Birkinshaw (1988); Davies & Illingworth (1983); Dressler & Richstone (1988); Dressler & Richstone (1990); Efstathiou *et al.* (1980); Efstathiou *et al.* (1982); Faber *et al.* (1989); Fisher *et al.* (1995); Franx *et al.* (1989a); Fried & Illingworth (1994); Gonzalez (1993); Jedrzejewski & Schechter (1988); Jedrzejewski & Schechter (1989); Kormendy (1982b); Kormendy (1988); Kormendy & Illingworth (1983); Kormendy & Richstone (1992); Kormendy & Westpfahl (1989); Scorza & Bender (1995); Tonry (1984); van der Marel *et al.* (1994); Whitmore *et al.* (1985); Young *et al.* (1978).
- Col. 6: Dimensionless ratio $(v/\sigma)_* \equiv \langle v/\sigma \rangle / \langle v/\sigma \rangle_{oblate}$ (see Davies *et al.* (1983) for definition). Most values have been taken from the literature; those calculated by us assume $\langle v/\sigma \rangle_{oblate} = [\epsilon/(1 - \epsilon)]^{1/2}$ from Bender (1988). Published sources of $(v/\sigma)_*$: Bender *et al.* (1992); Bender *et al.* (1994); Bosma *et al.* (1985); Davies *et al.* (1983); Fisher *et al.* (1995); Gonzalez (1993); Jedrzejewski & Schechter (1989); van der Marel (1991).
- Col. 7-8: Ellipticity and isophotal shape parameter, a_4/a ($\times 100$), as defined by Bender & Möllenhoff (1987). a_4/a is the coefficient of the cosine distortion term expressed as a percentage of major axis length. c_4 is also the cosine term but expressed as a percentage of surface brightness fluctuation around an elliptical isophote. a_4/a is related to c_4 by the local brightness gradient as follows:

$$a_4/a = c_4 \left| \frac{d \log I}{d \log r} \right|^{-1} (b/a)^{1/2},$$

where the second term corrects from the unit circle to the major axis (Bender *et al.* 1988). Where this formula is needed, we have simply taken $|d \log I / d \log r| = 2$ and ignored the second term. In estimating a_4/a from profiles, we have followed Bender *et al.* (1988) and used an average between $10''$ and $60''$. In the text, galaxies with $a_4/a > 0.4$ are classed as “disky” while all others (including irregular a_4/a ’s) are classed as “boxy”.

Sources for ϵ and a_4/a : Bender *et al.* (1989); Faber *et al.* (1989); Franx *et al.* (1989b); Goudfrooij *et al.* (1994); Jarvis & Freeman (1985); Kent (1983); Lauer (1985b); Lugger *et al.* (1992); Nieto *et al.* (1991c); Peletier *et al.* (1990); RC2; van den Bosch *et al.* (1994). For disk galaxies, we have attempted to find ϵ for the bulge only, but those for NGC 1023, NGC 2841, NGC 3384, and NGC 7332 are global axial ratios from the RC2.

- Col. 9: Profile class: \cap = core; \setminus = power law.
- Col. 10/12: Logarithm of break radii, in pc. Angular values from Table 1 (θ_b^{lim} and θ_b) have been converted to linear values (r_b^{lim} and r_b) using the distance in Mpc from Table 1. No cosmological curvature corrections have been applied.
- Col. 11/13: Break surface brightnesses μ_b^{lim} and μ_0 from Table 1 corrected for Galactic extinction (but not for K-correction or cosmological dimming).
- Col. 14-16: α , β , and γ from nuker-law fits, repeated from Table 1.
- Col. 17-18: Logarithm of the effective radius, in pc, and effective V-band surface brightness from Faber *et al.* (1989; NGC 1700 from Gonzalez 1993). $H_0 = 80 \text{ km s}^{-1} \text{ Mpc}^{-1}$ is assumed, and no cosmological curvature corrections have been applied. μ_e is the mean V-band surface brightness within r_e and is calculated from the B-band value in Faber *et al.* (1989) using $(B - V)_o$ from Table 1.